aerospace

MDPI

Review

Failure Mechanisms of Satellite Radio Frequency Modules in Extreme Environments: Challenges and Future Trends

Shuo Yan [1], Haoyi Wang [1] and Jianzhong Ding [2,*]

[1] School of Mechanical Engineering and Automation, Beihang University, Beijing 100191, China; yanshuo2002@buaa.edu.cn (S.Y.); sy2307106@buaa.edu.cn (H.W.)
[2] State Key Laboratory of Virtual Reality Technology and Systems, Beihang University, Beijing 100191, China
* Correspondence: jianzhongd@buaa.edu.cn

Abstract

Satellite communication greatly extends the reach and functionality of terrestrial communication networks, providing indispensable applications in defense, security, transportation, science, and technology. However, communication satellites operating in low Earth orbits face harsh space environments that severely affect their service life and reliability. The radio frequency (RF) module constitutes the core architecture of satellites, and its reliability directly determines overall satellite performance. While existing research has predominantly focused on the failure mechanisms of power amplifiers, investigations into the failure behaviors of other RF components—such as filters, frequency converters, and connectors—remain comparatively fragmented. Moreover, a comprehensive and systematic review addressing the RF module from a holistic, cross-component perspective is notably absent in the current literature. Therefore, this study comprehensively reviews existing studies on the reliability of spaceborne electronic components, highlighting both commonalities and differences in their failure mechanisms. Particular attention is given to in-orbit failure mechanisms of critical components, including power amplifiers, frequency converters, filters, and RF connectors. From the perspective of electronic components, this study assesses the in-orbit service capability, reliability, and lifespan of communication satellites. Finally, it identifies key challenges in ensuring the reliability of satellite electronic components and proposes future research directions and technical strategies for improvement. This study provides systematic insights for researchers in satellite communication RF modules and establishes a foundation for further advancements in the field.

Keywords: spaceborne electronic devices; failure mechanisms; extreme environment; satellite communication

Check for updates

Academic Editor: Paolo Tortora

Received: 12 March 2026
Revised: 29 April 2026
Accepted: 3 May 2026
Published: 7 May 2026

Copyright: © 2026 by the authors. Licensee MDPI, Basel, Switzerland. This article is an open access article distributed under the terms and conditions of the Creative Commons Attribution (CC BY) license.

1. Introduction

In recent years, communication satellites have been increasingly integrated into future wireless networks [1], and higher demands have been placed on transmission speed and coverage. To satisfy these requirements, satellites are evolving toward multifunctionality [2], leading to the deployment of remote sensing, broadcasting, communication, and navigation satellites. Their systems are moving in the direction of high bandwidth, strong integration, and progressive miniaturization (Figure 1) [3]. Compared with terrestrial wireless technologies, satellite communication operates beyond Earth's atmosphere, thereby achieving superior stability, cost efficiency, and extensive coverage across a wide geographical area. Consequently, it has been widely adopted in national defense, military operations, transportation, water resource management, and emergency rescue missions [4,5].

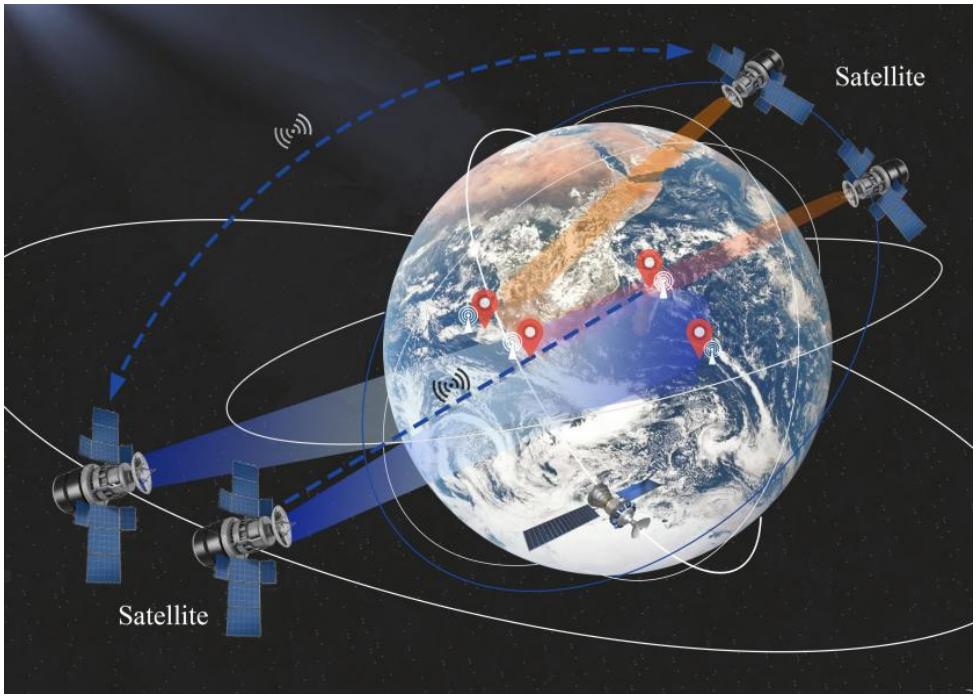


Figure 1. Satellite communications in orbit.

Radio frequency (RF) integrated circuits represent the most critical components within these systems, as their performance determines both reliability and service life. However, satellites must operate continuously in harsh space environments, which are defined by resource scarcity (power limited to solar panels), intense radiation (including solar radiation, galactic cosmic rays, and Earth's magnetic field) [6], high vacuum [7], microgravity with potential impacts from high-velocity particles [8], and extreme temperature fluctuations [9]. These conditions prevent ground stations from accurately monitoring the real-time status of electronic components and make the timely replacement of faulty parts virtually impossible. Such constraints present major challenges for sustaining the operational lifespan of space terminals.

The combined impact of these environmental factors may frequently cause component malfunctions, leading to communication link failures, service interruptions, and performance degradation. This issue is especially critical for 6G terahertz communication. Consequently, developing effective monitoring and reliability enhancement strategies for spaceborne RF modules under extreme environmental conditions has become a central challenge in advancing satellite communication technology. The application of RF devices to satellite communication systems is shown in Figure 2.

In recent years, extensive research has been conducted on satellite communication technology and spaceborne RF electronic components. Within the field of satellite communication, Al-Hraishawi et al. [10] conducted a comprehensive survey on non-geostationary orbit (NGSO) satellites, focusing on their technical advantages and communication prospects. Their analysis encompassed the physical layer, radio access technologies, system architecture, and overall network functionality. They also addressed key challenges, including coexistence with geostationary orbit (GSO) systems in terms of spectrum access and regulation, satellite constellation and architecture design, resource allocation, and requirements for user equipment. Su et al. [11] presented a systematic discussion of the core elements of broadband low Earth orbit (LEO) satellite communication systems. They described a space-based architecture integrated with inter-satellite links (ISL) and introduced two representative constellations, Walker Delta and Star, along with wide-beam and spot-beam

coverage strategies for seamless global service. Satellite quantum communication, regarded as a core technology for quantum key distribution (QKD) and quantum state transmission, has emerged as an important research direction. Agnesi et al. [12] summarized the most recent advances and analyzed observable phenomena associated with existing techniques. Building on this, Sodagari et al. [13] examined the synergy between quantum technologies and satellite communications. They discussed continuous-variable and discrete-variable QKD schemes, evaluated optimal orbital strategies for QKD satellites, and emphasized the role of quantum computing in enhancing the security of satellite information networks. Multiple-input multiple-output (MIMO) technology, which employs multiple transmitting and receiving antennas, has significantly advanced high-speed mobile communication and facilitates global wireless access at higher data rates. Building on the two pillars of fixed and mobile satellite communications and considering the specific characteristics of satellite channels, Arapoglou et al. [14] conducted a detailed review of MIMO-based technologies in satellite communication systems and examined their feasibility for practical applications. As the openness of satellite communication channels poses significant risks to national and personal privacy, covert satellite communication technologies have been proposed to enhance system concealment. Lu et al. [15] summarized the current state of key technologies in covert communication and demonstrated the integration of artificial intelligence (AI) in this domain. In the field of spaceborne RF components, Luo et al. [16] reviewed the role of microwave vacuum electronic devices in RF modules, highlighting the inherent advantages of such devices in supporting high-power and high-power density.

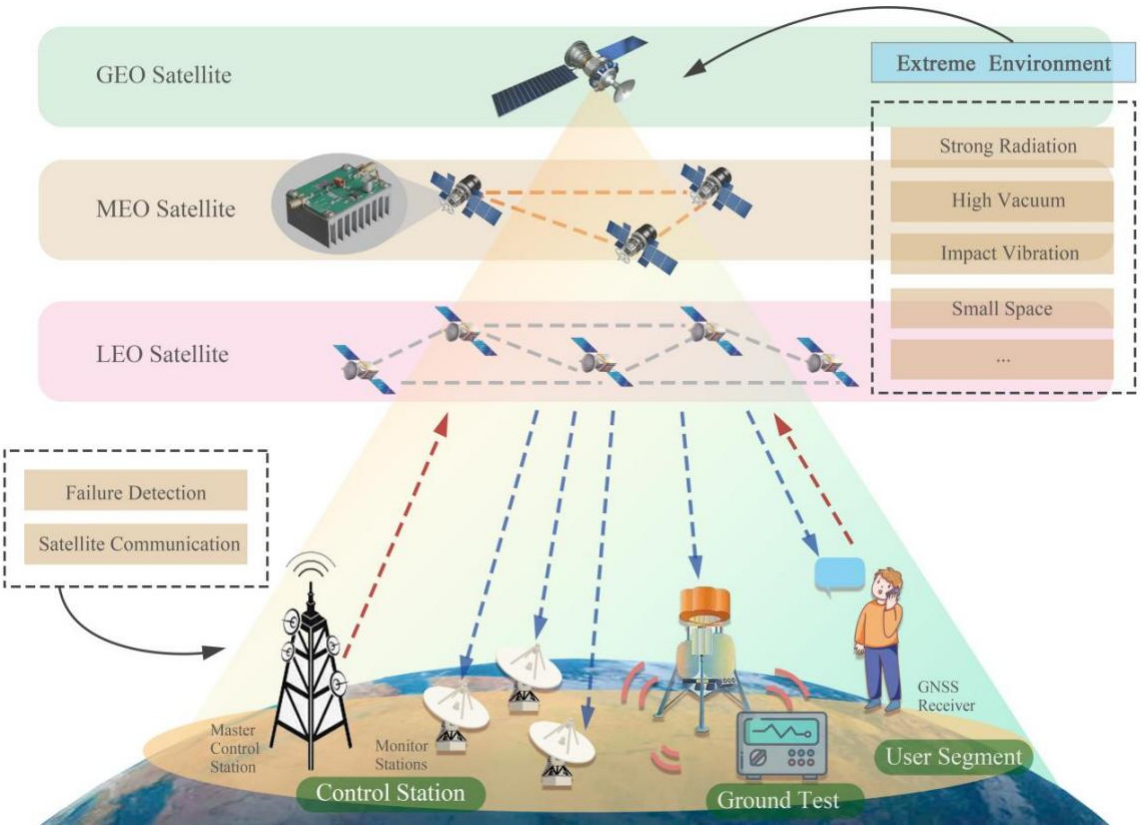


Figure 2. Application of radio frequency modules in satellite communication technology.

The aforementioned studies mainly reviewed cutting-edge technologies in satellite communication and optimization of mechanical structures. Nevertheless, research specifically addressing the failure mechanisms and reliability analysis of electronic components in extreme space environments remains limited despite these components serving as the core

architecture. To bridge this gap, this study examines the current domestic and international research status of core spaceborne RF components at both domestic and international levels, starting from studies of failure mechanisms. On this basis, this study systematically summarizes typical on-orbit failure causes and phenomena observed in components such as power amplifiers, frequency converters, filters, and RF connectors operating under extreme space conditions. Furthermore, it explores the development trends of reliability enhancement and fault detection technologies, aiming to provide technical support for extending the service life of 6G communication terminals carried by satellites.

2. Failure Modes and Mechanism Analysis of Spaceborne Electronic Components

Prior to the launch of communication satellites, RF equipment should undergo a series of qualification tests prescribed by aerospace agencies to demonstrate its feasibility under extreme temperature, power handling, and mechanical stress conditions [17]. However, ground-based testing cannot fully replicate the actual in-orbit environment and therefore fails to accurately capture real failure mechanisms. This review focuses on the analysis of failure modes observed in spaceborne RF components during in-orbit operation. The discussion includes high-power amplifiers, input–output multiplexing filters, digital frequency converters, and cable assemblies. These devices commonly experience dynamic nonlinear effects, input-related anomalies, and mechanical damage. Such problems may result in RF module malfunctions and cause severe degradation of the quality of the transmitted signals. The major categories of core spaceborne electronic components examined for failure mechanisms in this study are illustrated in Figure 3.

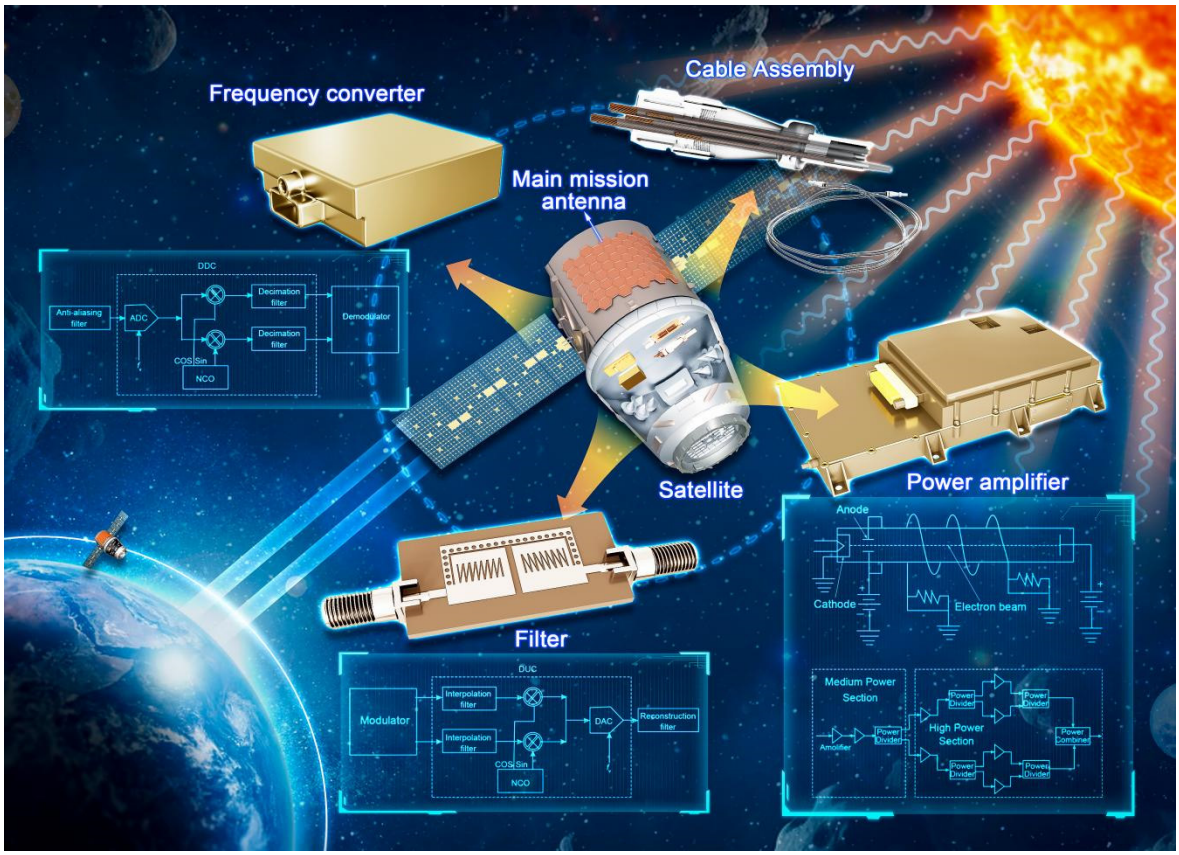


Figure 3. General schematic diagram of satellite-borne electronic components.

2.1. Analysis of Common Failure Phenomena of Spaceborne Electronic Components

In satellite communication systems, the failure modes of spaceborne electronic components exhibit notable common mechanisms that primarily originate from extreme space environments. The classification of these mechanisms is illustrated in Figure 4.

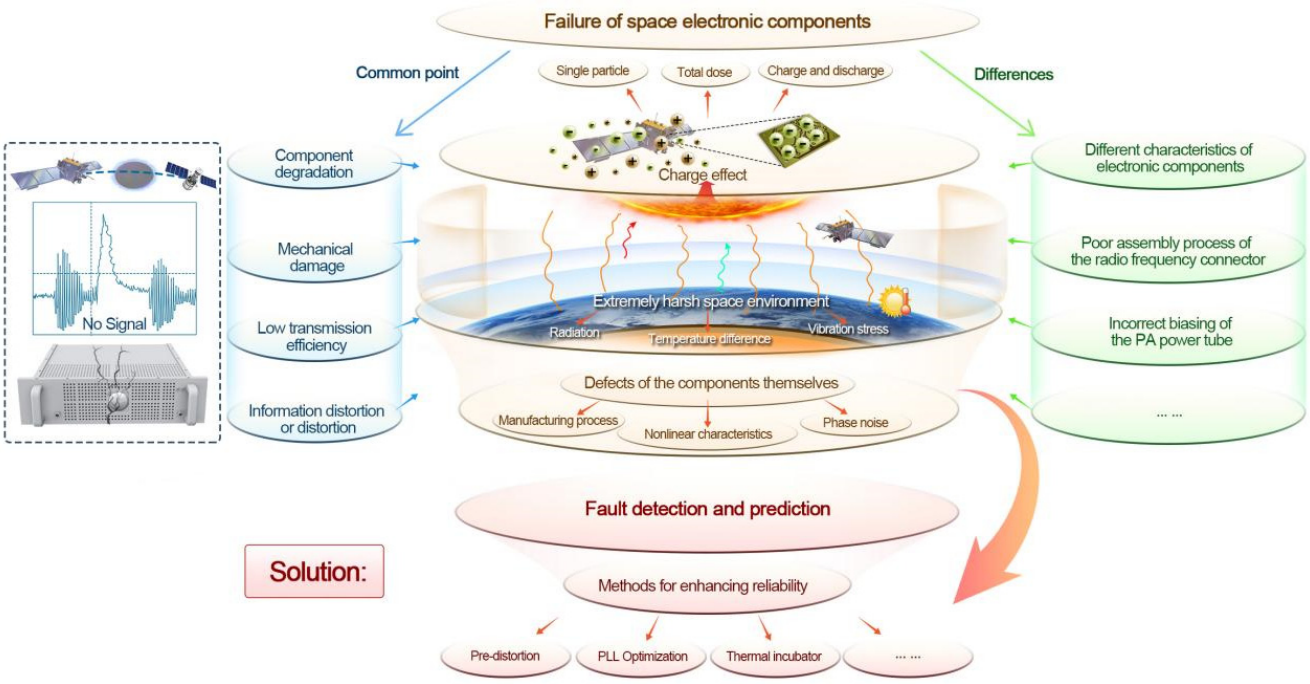


Figure 4. Classification of failure mechanisms of spaceborne electronic components.

2.1.1. Fundamental Physical Failure Mechanisms Induced by the Space Environment

(1) Micro-discharge effect

The micro-discharge effect was first observed in Ku-band satellite transmitters in 1997. Since then, it has also been reported in other Ku-band systems, as well as in Ka-band and S-band traveling-wave tube amplifiers on various satellites [18], which have attracted significant attention. This effect occurs when free electrons ionized in a vacuum are accelerated by an externally applied RF field, producing secondary electron multiplication, which eventually leads to an avalanche process [19]. The essential conditions for its occurrence include (1) a vacuum environment, (2) the presence of free electrons, and (3) a secondary electron transit time equal to an odd multiple of half the RF signal period. Because spaceborne components typically operate under high voltages, these conditions are almost always satisfied, resulting in distortion or outright failure. Therefore, the prevention of micro-discharge has become a major challenge in the design of RF devices. Figure 5 illustrates the region between the parallel plates where micro-discharges can be observed.

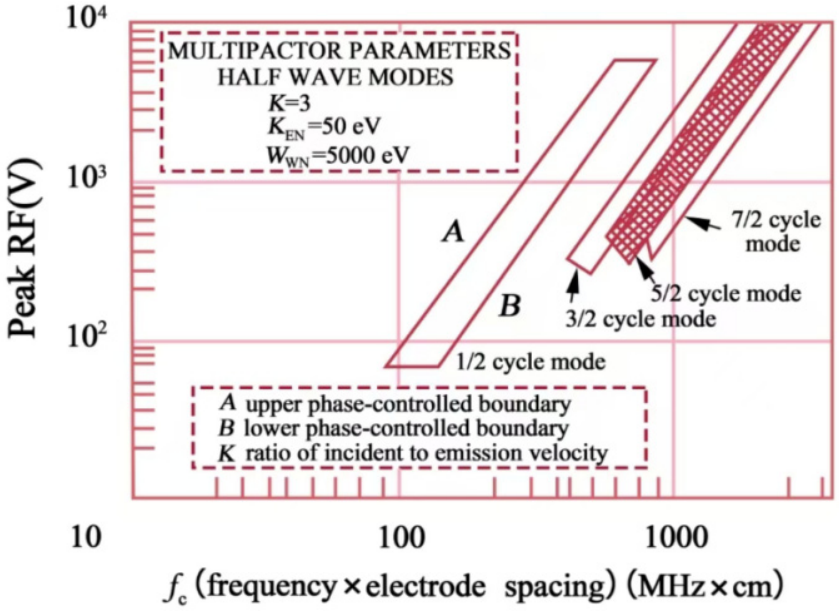


Figure 5. Areas between parallel plates where micro-discharges may occur.

Considering the composite transit-time model, the analysis begins with the electron motion equation between the two parallel plates:

$$\mathrm{m}\frac{\mathrm{d}^2x}{\mathrm{d}t^2} = \mathrm{eEsin}(\omega t + \varphi), \tag{1}$$

The final-stage integration of Equation (1) yields the terminal voltage V_f at which an electron reaches the opposite plate:

$$V_f = \frac{k}{k-1} \times \frac{2eE}{\mathrm{m}}\cos\varphi, \tag{2}$$

where φ is the phase angle at which secondary electron emission occurs; m and e are the mass and charge of the electron, respectively; and $k = V_f/V_s$ is the ratio of the electron's terminal voltage to its emission voltage (a constant) [20].

The second integration of Equation (1) provides the breakdown voltage V for secondary electron multiplication:

$$V = \frac{4\pi^2(f \times d)^2}{(\mathrm{e}/\mathrm{m})\Phi}, \tag{3}$$

$$\Phi = \frac{k+1}{k-1}(2n-1)\pi\cos\varphi + 2\sin\varphi, \tag{4}$$

where k and φ are constants; f is the operating frequency; and d is the distance between the two plates (i.e., the gap size). Equation (3) indicates that the breakdown voltage V is directly proportional only to the product $f \times d$. Because operating frequency f is fixed by the mission, the gap size d is the only parameter positively correlated with the micro-discharge threshold.

To increase this threshold, gaps in the circuit should ideally be eliminated to prevent electron motion and multiplication. However, such modifications inevitably increase both the volume and the weight of the device. From the perspective of the necessary conditions for micro-discharge, the electron motion under the applied RF field is the critical factor driving electron multiplication. According to the diffusion breakdown mechanism of microwaves,

$$F = \mathrm{m_e}a = \mathrm{m_e}\frac{\mathrm{d}\nu_\mathrm{e}}{\mathrm{d}t} = q_\mathrm{e}E_0\cos\omega t, \tag{5}$$

where F is the electromagnetic force; m_e, q_e, a, and v_e are the mass, charge, acceleration, and instantaneous velocity of the electron, respectively; E_0 is the electric field strength; and ω is the frequency. After integration, the electron motion distance L in the field is expressed as:

$$v_e = \frac{E_0 q_e}{m_e \omega} \sin \omega t, \tag{6}$$

$$L = \int_0^{T/2} v_e dt = \frac{E_0 q_e}{m_e \omega} \int_0^{T/2} \sin \omega t dt = \frac{2E_0 q_e}{m_e \omega}, \tag{7}$$

where q_e/m_e is a constant equal to 1.76×10^{11} C/kg.

When the electron motion distance L exceeds the internal gap size d, and the transit time corresponds to an odd multiple of half the RF period, micro-discharge is readily triggered. Because the gap size d is constrained by circuit design and device miniaturization, it cannot be arbitrarily removed or increased. As a result, the motion distance L of electrons becomes the decisive factor in determining whether micro-discharge occurs. Equation (7) shows that with q_e/m_e and ω constant, L depends only on E_0. Therefore, reducing the internal electric field strength E_0 is the key to suppressing micro-discharge and raising the threshold for its onset.

(2) Total ionizing dose effect and single-event effect

High-energy particles in near-Earth space primarily originate from Earth's radiation belts, solar radiation, and cosmic rays. These particles can significantly affect digital circuits, particularly integrated circuits, and represent a major source of potential failure for spaceborne electronic components. Their influence is mainly manifested in two forms: the total ionizing dose (TID) effect and the single-event effect (SEE) [21].

The TID effect is cumulative and results from the absorption of ionization energy by charged particles. When γ photons or high-energy ions penetrate the circuit material, they generate electron–hole pairs. These pairs subsequently recombine, diffuse, and drift, leading to the accumulation of oxide trap charges in the oxide layer or interface trap charges at the boundary between the oxide layer and the semiconductor material. The resulting process degrades device performance and may ultimately lead to functional failure.

In contrast, SEE is a transient phenomenon. When a high-energy particle traverses a sensitive region of a circuit, localized ionization can induce circuit malfunctions. Based on the observed behavior, SEE can be classified into several types, as listed in Table 1.

Table 1. SEE types.

Type	Definition
Single-event upset (SEU)	A high-energy particle alters the logic state of the device
Single-event functional interrupt (SEFI)	A particle induces functional anomalies in a device
Single-event latch-up (SEL)	A parasitic thyristor effect triggered in CMOS devices
Single-event burnout (SEB)	Commonly occurs in power amplifiers under space radiation, where power transistors are irreversibly damaged by breakdown
Single-event gate rupture (SEGR)	A high-energy particle causes the breakdown of the gate insulation

These faults may be recoverable or permanent [22–25]. SEU and SEFI generally cause temporary changes, such as altering memory cell states or introducing transient

interference signals, which can often be mitigated by resetting the device. In contrast, SEL, SEB, and SEGR typically result in irreversible transistor damage, causing the device to cease functioning entirely.

With ongoing advances in electronic design and integration, the tolerance of integrated circuits to high-energy particles has been significantly improved. Consequently, the likelihood of permanent damage caused by TID or SEE is substantially reduced. Currently, additional protective measures are seldom required because the probability of such failures is much lower than the intrinsic failure rate of the components. Consequently, TID and SEE are no longer considered primary failure concerns. A schematic illustration of these effects is shown in Figure 6.

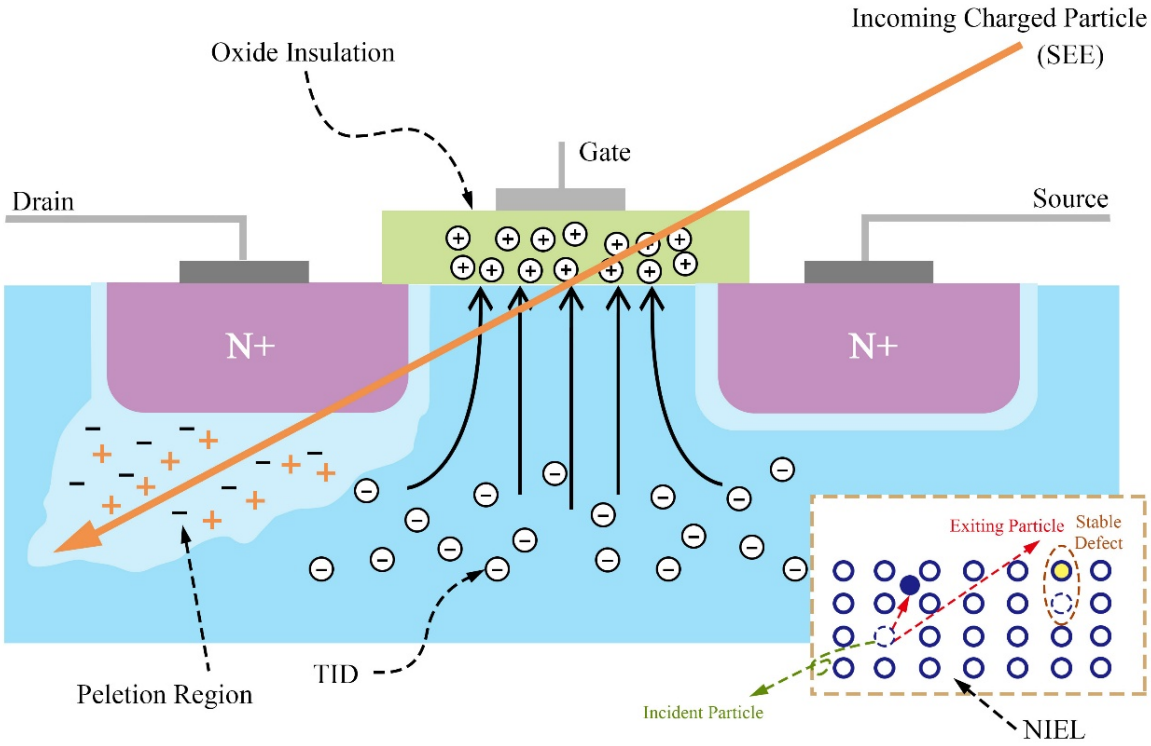


Figure 6. Single particle and total dose effects.

(3) Charging and discharging effect

A harsh high-energy electron environment frequently induces failures and anomalies associated with satellite charging and discharging. The resulting current pulses and electromagnetic fields can propagate and couple into satellite equipment through multiple pathways, such as circuits or free space, ultimately producing "soft error" failures similar to spaceborne SEEs.

In outer space, plasmas composed of electrons, environmental electrons, and secondary electrons interact with satellite surfaces owing to their charge-carrying nature and high conductivity. This interaction may cause negative charge accumulation either on the satellite surface or within spacecraft materials. Under particle bombardment, secondary electrons are released, whereas solar illumination induces photoelectron emission. When the potential difference exceeds a threshold value, charging and discharging occur. These events may result in material degradation, electrostatic discharge (ESD) damage, or electromagnetic interference with onboard equipment. A schematic illustration of the surface charging and discharging effects is provided in Figure 7.

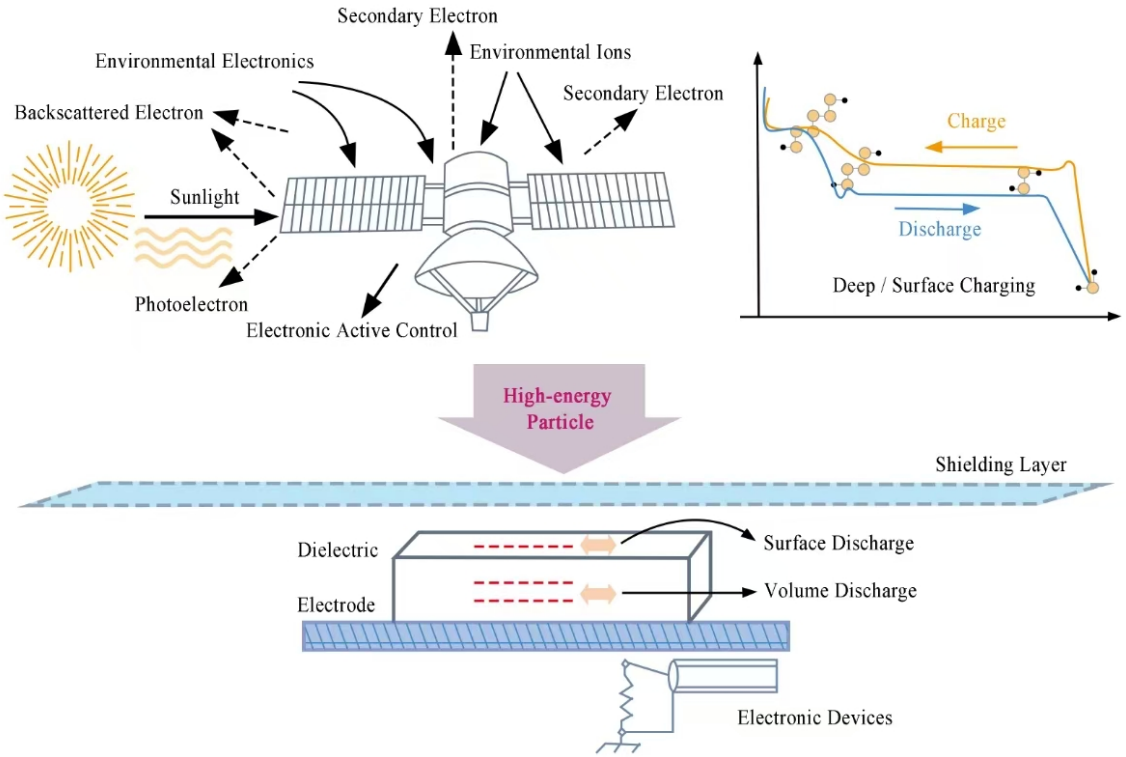


Figure 7. Charging and discharging effects.

Enhanced solar activity, such as high-speed solar wind streams, intensifies these processes by significantly increasing the flux of high-energy electrons from several hundred keV to several MeV by several orders of magnitude. In addition to causing charging and discharging on satellite surfaces, such electrons can penetrate deeply into dielectric materials, leading to severe internal damage and functional degradation of electronic equipment. To mitigate these risks, international standards generally require protective design measures for charging and discharging. However, current technologies remain suboptimal and continue to exhibit deficiencies, leaving residual risks of interference and failure in practical applications.

(4) Component degradation or mechanical damage

During in-orbit operations, extreme environmental factors frequently cause degradation and mechanical damage to spaceborne electronic components. A high vacuum in orbit (less than 10^{-6} Pa) leads to the disappearance of oxide films on metal surfaces, resulting in a general reduction in the component lifespan compared with terrestrial conditions. In addition, damage from radiation belts, uneven thermal expansion induced by severe temperature cycling [26–28], amplified random loads and impacts under microgravity conditions (which may cause resonance in severe cases), and collisions with space debris (with an average impact speed of 20 km/s) all pose serious threats to device integrity. Despite the adoption of new composite materials and advanced structural topology optimization methods aimed at extending service life, the outcomes often fall short of expectations. Consequently, mechanical damage and component degradation caused by extreme environments remain common issues that require close attention [29].

Radiation is among the most destructive factors affecting spacecraft. Radiation-induced mechanical damage can be broadly categorized into ionizing damage and displacement damage. Ionizing damage occurs when incident particles ionize target atoms and excite extranuclear electrons within the material, producing electron–hole pairs. On the other hand, displacement damage occurs when incident particles interact with atoms in the

material, exchange kinetic energy, and displace atoms from their original lattice positions. This process generates interstitial atoms and vacancies, and displaced atoms may undergo successive collisions with surrounding atoms, leading to displacement cascades.

2.1.2. Functional Failures in Generic Components

(1) Signal distortion or deformation

Signal distortion or deformation represents a particularly prominent type of malfunction. The internal or inter-component electrical signals of high-power RF devices are highly complex, involving both high- and low-frequency circuits, as well as digital and analog subsystems. Owing to structural constraints, physical isolation between circuits is difficult to achieve, which intensifies superimposed interference effects. Under extreme conditions, such as severe temperature cycling and strong radiation in the space environment, components with different electrical characteristics may experience chain failure. These include surface ionization damage and network tuning mismatches. For instance, in RF links, impedance discontinuities in connectors, cables, or PCB traces may lead to signal reflection, thereby generating standing waves and echo loss. A representative satellite navigation signal distortion model is shown in Figure 8. Signal distortion can generally be divided into digital distortion and analog distortion, with digital distortion commonly described using the classical TMA model.

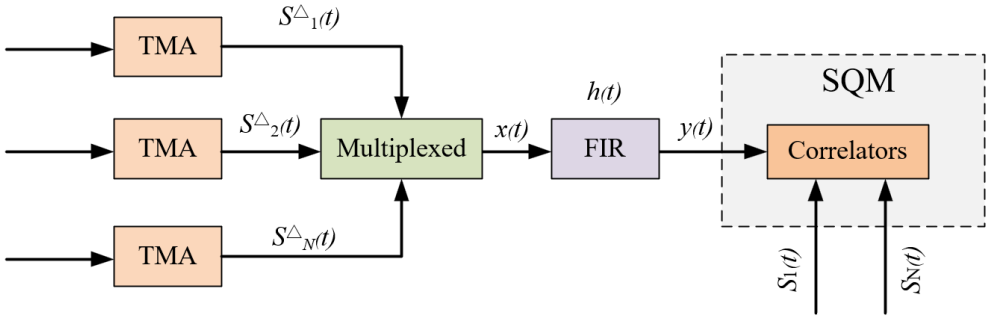


Figure 8. Signal distortion modeling for satellite navigation communications [30].

Although signal distortion or deformation is widely observed, the mechanisms and primary causes of failure vary depending on specific influencing factors. In the following sections, these failures are examined individually, focusing on the unique characteristics of different electronic components.

(2) Low output power

Low output power is another common failure mode in spaceborne RF components, and similar to signal distortion, results from the combined influence of multiple factors. Although the manifestation is consistent, the underlying causes differ. This may arise from the nonlinear characteristics inherent in spaceborne devices, extreme environmental stresses, output load variations, or impedance mismatch in the network. When such degradation is detected, the initial diagnostic step is to verify whether the frequency and impedance of the input signal fall within an acceptable range. If a mismatch is identified, adjustments should be implemented promptly to prevent component damage. If the input signal matches the component specifications, the analysis should consider the intrinsic device characteristics combined with the extreme temperature and surface radiation conditions to which the component is exposed. Only through this combined evaluation can the underlying mechanism of low output power be accurately identified.

2.2. Power Amplifier

A spaceborne power amplifier (PA) is responsible for amplifying the communication signal power of satellites to ensure effective transmission to the ground or to other satellites. Typically, the PA is located at the transmitting end of the satellite communication system, where the signal is first processed through the modulator, frequency converter, and band-pass filter before being amplified to the required power level for transmission. Power amplifiers are indispensable in RF circuits, with performance indicators such as stability, gain flatness, linearity, and output power directly influencing transmitter performance and overall signal quality. Under in-orbit conditions, failures can be frequently identified, including low output power, distortion or deformation, load overheating, and mechanical faults. Several space missions have reported cases of satellite power amplifier failures [31]. For example, the Galileo GSAT-0104 and GlobalStar satellite constellations, which operate in the radiation environment of medium Earth orbit, experience a gradual decline in power until failure. The internal schematics and failure mechanisms of the PAs are shown in Figure 9.

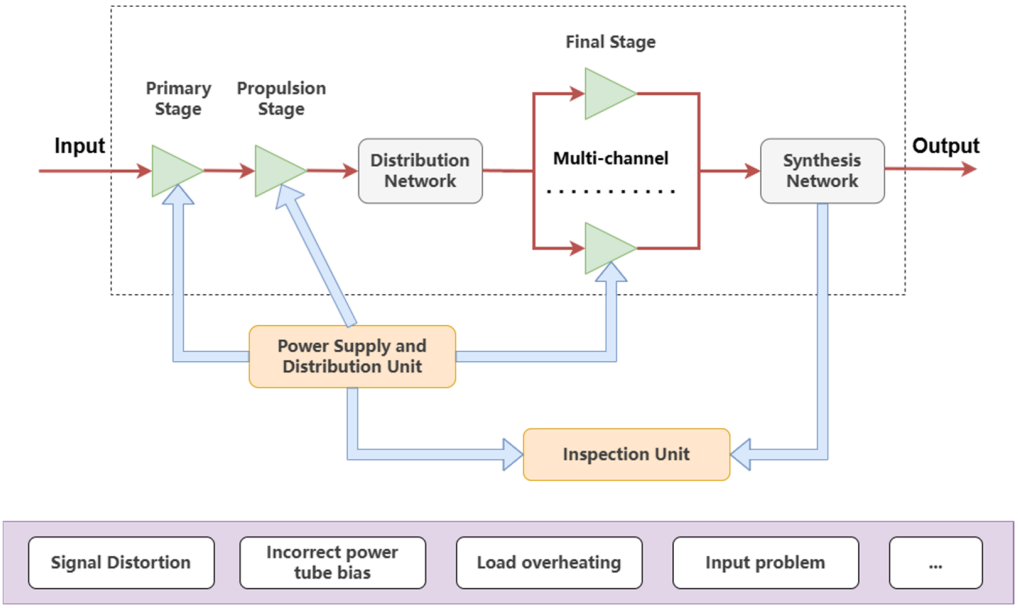


Figure 9. Electrical principles and causes of failure of spaceborne power amplifiers.

With the increasing demand for high-speed transmission and a broader bandwidth capacity, the K/Ka-band, with its wide available bandwidth (26.5–40 GHz) and relatively low interference, has gradually become the dominant choice for high-capacity satellite systems [32]. Accordingly, this review focuses on analyzing the failure mechanisms of power amplifiers used in Ka-band satellite communications.

Historically, high-power spaceborne amplifiers have primarily relied on vacuum electronic devices, particularly traveling-wave tube amplifiers (TWTAs). In contrast, semiconductor-based amplifiers have mainly been employed for medium- and low-power applications. In recent years, various semiconductor processes have proven to be effective for Ka-band systems. These include gallium arsenide pseudomorphic high electron mobility transistors (GaAs pHEMTs) [33], gallium nitride high electron mobility transistors (GaN HEMTs) [34], indium phosphide heterojunction bipolar transistors (InP HBTs) [35], silicon complementary metal–oxide-semiconductor (Si CMOS) [36], silicon and germanium bipolar complementary metal–oxide-semiconductor (SiGe BiCMOS) [37,38], and silicon on insulator complementary metal–oxide-semiconductor (SOI CMOS) [39–41]. In the past, semiconductor devices were predominantly based on silicon. With growing

demands for higher performance, high electron mobility transistor (HEMT) structures using AlGaAs/GaAs crystals were developed in the late 1970s and the early 1980s. As a representative material, GaAs has gradually replaced Si in these applications. However, the AlGaAs/GaAs heterojunction contains a deep donor state known as the DX center, which can degrade the performance of electronic devices under low-temperature conditions [42]. To address these limitations, indium phosphide (InP), which is widely used in HEMT and HBT processes, as well as mature CMOS technology, was subsequently introduced.

In summary, for devices operating at frequencies below 100 GHz, GaN and GaAs remain advantageous owing to their superior output powers. For ultra-high-frequency applications exceeding 500 GHz, InP-based devices are more suitable, particularly for high-power amplifiers. In contrast, when cost is the primary consideration in industrial production, CMOS continues to be the preferred option because of its advantages in system-on-chip integration. Another promising development direction lies in passive component integration.

2.2.1. Low Output Power or Impedance Mismatch

As high-power electronic devices, spaceborne power amplifiers are highly sensitive to variations in the output load, and failures are frequently caused by these fluctuations [43]. This is particularly evident in final-stage power amplifiers, where inherent nonlinearity under high input/output loads results in impedance disturbances and intermodulation distortion. When operating in the saturation region, the dynamic change in the output impedance with power becomes more pronounced than that in other electronic components. In severe cases, this may result in a reverse flow of reflected energy, potentially damaging the amplifier. Cascading a power amplifier directly with a filter can increase the risk of an impedance mismatch [44]. A low output power is closely associated with losses in the output matching network. This effect is particularly significant in high-frequency, high-power scenarios, where large amounts of output energy are dissipated. Therefore, current improvement strategies emphasize increasing the optimum load impedance and reducing the impedance transformation ratio, which lowers ohmic losses and current stress within the matching network. Such measures effectively minimize dissipation and improve overall efficiency [45].

In addition, as active devices, power amplifiers also experience degradation of their band structures, which constitutes another key mechanism for reduced output power. At GaN gates, the reverse piezoelectric effect induces lattice defects and unconventional geometric deformation. This phenomenon produces more severe consequences than other semiconductor devices, rendering it essential to address both micro-discharge suppression and the mitigation of reverse piezoelectric effects in GaN-based amplifiers.

2.2.2. Nonlinear Distortion

Signal transmission should satisfy three primary technical requirements, including spectral bandwidth expansion, transmission power enhancement, and efficiency improvement. In striving to meet these goals, the nonlinear characteristics of electronic components become unavoidable because they frequently give rise to nonlinear distortion. Power amplifiers exhibit the most pronounced nonlinear behavior owing to their high-power consumption. Because inductors and capacitors within the circuit possess storage functions, the instantaneous voltage and current at each node depend not only on the present input but also on historical values. This memory effect causes intermodulation distortion when the input signal power becomes excessive because nonlinear responses alter the composition of the output signals. In addition to memory effects, nonlinear gate-drain capacitance

(CGD) and drain–source capacitance (CDS) are the contributors to poor linearity in RF CMOS power amplifiers [46].

Nonlinear distortion of power amplifiers is generally classified into two types: in-band distortion (AM/AM) and out-of-band distortion (AM/PM). In-band distortion manifests as amplitude and phase cross-modulation in the output signal, which is commonly mitigated through adaptive biasing, linearization, and gm-compensation techniques. Out-of-band distortion originates from regenerated harmonic components, leading to adjacent-channel interference. In practical wideband multi-carrier systems, these two forms of distortion frequently coexist, resulting in complex time–frequency coupling characteristics.

2.2.3. Driven to Saturation Point

Power resources on satellites are extremely limited. To maximize power utilization and reduce energy consumption, amplifiers often operate near their saturation points. However, this intensifies the nonlinear interactions between the electron beam and slow-wave structures in TWTAs [47]. In addition, I–V curve bending caused by transconductance compression of GaN/GaAs transistors in solid-state power amplifiers (SSPAs) may induce severe signal distortion. When the input amplitude approaches the saturation threshold, higher-order modulated constellation points may rotate, compress, or even overlap [48]. Furthermore, in multi-carrier systems, nonlinearities can generate third-order intermodulation products that fall within the communication band, thereby creating an in-band noise floor that is difficult to eliminate. Fifth-order and higher intermodulation products may also extend into adjacent bands, violating out-of-band emission limits set by the International Telecommunication Union [49].

2.2.4. Incorrect Biasing of Power Transistors

The operational stability of spaceborne amplifiers depends critically on active biasing. Incorrect biasing not only leads to performance degradation but may also cause single-point failures such as GaN gate breakdown or collector melting, resulting in power supply overload. This issue stems from the interaction between nonlinear effects triggered by bias point deviation and intrinsic characteristics of the device. In practice, spaceborne amplifiers typically operate continuously, with a fixed bias voltage applied to their transistors. If the static bias voltage or current deviates from the optimal setting, the transistor exits its intended region of operation, disrupting the linear mapping between input and output signals. For instance, GaN transistors commonly used in SSPAs are extremely sensitive to gate bias. When the bias is set too high, transistors enter saturation prematurely, compressing the high-amplitude portions of the input signal (AM-AM distortion) and reducing channel carrier mobility, which induces phase delay (AM-PM distortion). This leads to a constellation rotation and amplitude compression. Conversely, when the bias is too low, transistors operate in a weak conduction state near the cutoff, producing crossover distortion, where low-amplitude signals are clipped, and waveform distortion occurs.

Thermal effects further exacerbate these problems. Excessive current mismatch can increase junction temperature, shorten device lifetime, and degrade reliability. The thermal–electrical feedback mechanism amplifies these failures. In TWTAs, incorrect biasing (such as collector voltage deviation) reduces electron beam efficiency in the slow-wave structure, thereby lowering output power and triggering cascading system failure. Harmonic components generated under such conditions, such as second-order ($2f_0$), third-order ($3f_0$), and intermodulation products, accumulate and are amplified over the long satellite-to-ground transmission path, severely reducing the signal-to-noise ratio and error vector magnitude. Additionally, temperature fluctuations in orbit can cause bias drift (e.g., GaN threshold voltage decreases with increasing temperature). Without effective compensation

mechanisms, the static operating point shifts, forcing nonlinear distortion to vary with time–frequency conditions. Conventional predistortion algorithms cannot adequately track these dynamic variations, often leading to amplifier control failure and eventual communication interruption. The PA dynamic bias circuit is shown in Figure 10.

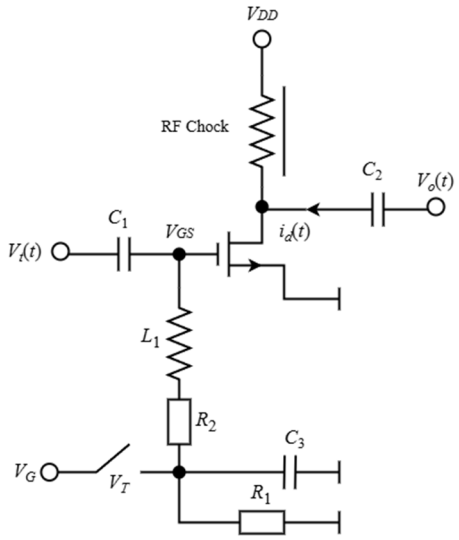


Figure 10. Power amplifier dynamic bias circuit.

Both domestic and international research have provided detailed examinations of how the efficiency and linearity of power amplifier transistors can vary with the bias voltage. Reported methods include envelope modulation of gate bias [50], control of drain voltage and current [51], dynamic adjustment of input and output bias voltages [52], simultaneous optimization of bias and RF power through combined consideration of drain voltage and RF input [53], and the application of DC-DC converters for input signal predistortion, power supply voltage optimization, and equalization [54].

Therefore, precise control of power transistor biasing requires the integrated optimization of temperature sensor feedback, adaptive bias circuits, and predistortion models, with the objective of achieving a balance between efficiency and linearity.

2.2.5. High-Spectral-Efficiency Modulation Schemes

To improve communication rates and spectral utilization, modern satellite communication systems have increasingly adopted high spectral-efficiency modulation schemes, such as quadrature amplitude modulation (QAM), orthogonal frequency-division multiplexing (OFDM), and their combinations with non-orthogonal multiple access technologies. Unlike constant-envelope signals, the signals generated by these complex modulation schemes typically exhibit a high peak-to-average power ratio (PAPR). When amplified using conventional linear power amplifiers, the average efficiency is relatively low [55]. If a spaceborne power amplifier operating in saturation is employed, its nonlinear characteristics can strongly interact with the modulated signals, producing a severe nonlinear distortion in the output.

The amplitude of non-constant-envelope modulation signals varies dynamically with each symbol and is closely coupled with the nonlinear transfer function of the amplifier. This sensitivity to amplitude fluctuations results in signal compression, phase distortion, and weakened low-amplitude signals, whereas high-amplitude signals suffer from compression in the saturation region. Consequently, constellation rotation, symbol overlap, and degradation of error vector magnitude (EVM) can be observed. In multi-carrier scenarios, dynamic amplitude variations induce dense intermodulation distortion (e.g., third-order

IMD), forming an in-band noise floor and broadening signal bandwidth. Phase–amplitude coupling further destabilizes demodulation performance, making it highly susceptible to random phase deviations. These deviations blur symbol decision boundaries and, in severe cases, cause synchronization loss. Thus, the statistical properties of non-constant-envelope modulation aggravate the asymmetric distortion in power amplifiers.

For high-PAPR signals, the large difference between instantaneous peak and average power forces amplifiers to operate in a deeply nonlinear saturation region [56]. This condition produces hard clipping, which flattens waveforms, generates higher-order harmonics, and causes spectral regrowth. As a result, the adjacent-channel leakage ratio (ACLR) deteriorates, potentially violating ITU spectrum mask requirements. Although power back-off can suppress clipping effects, it significantly reduces amplifier efficiency and increases energy stress. In addition, the wideband nature of high-PAPR signals stimulates memory effects, leading to time-domain distortion and inter-symbol interference [57]. Traditional predistortion algorithms struggle to compensate for these nonlinearities. The core issue lies in the trade-off between PAPR reduction and dynamic range, which creates energy efficiency imbalances in satellite links. Further exploration of hybrid linearization techniques, including balancing efficiency and back-off, may offer improved solutions. As illustrated in Figure 11, reference [56] proposed a digital power amplifier combined with a signal optimization control technique for OFDM signal amplification. In this approach, the input amplitude-modulated signal is quantized into $2^3 = 8$ states, which are used to control three power-scaled amplifiers. The outputs are then combined to reconstruct the quantified envelope signal.

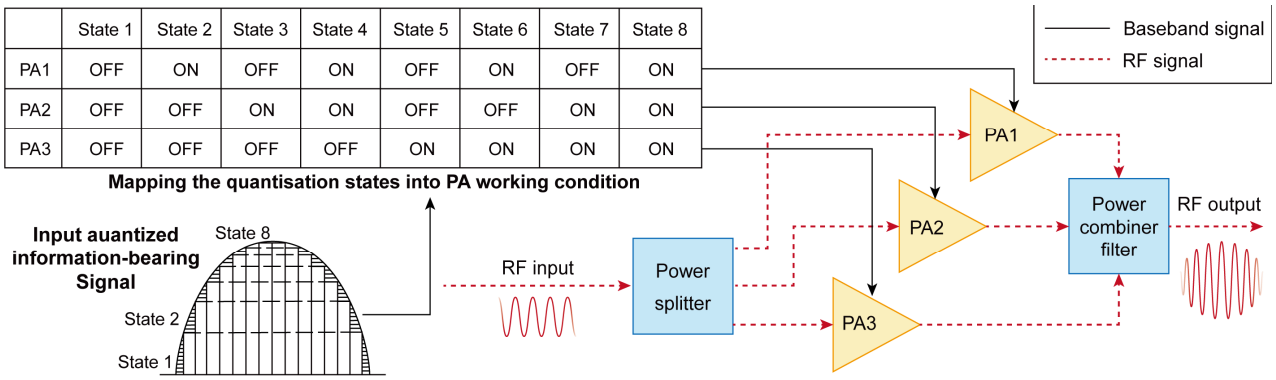


Figure 11. Block diagram of the proposed 3-bit DPA [58]. A constant-envelope phase-modulated RF input signal is fed to a three-way power combiner that splits the signal into three PAs.

2.2.6. High-Power Density Heat

On-orbit failures caused by overheating or overload due to high-power density heat are among the most critical issues in spaceborne high-power amplifiers. These failures are closely related to the complex circuit characteristics and high-power operation of the amplifiers, which are often aggravated by inadequate thermal design or excessive input signals.

In spaceborne power amplifiers, the core transistors of each amplification stage are the primary heat-generating devices, with the final-stage high-power transistors representing the most significant heat sources. Under nominal operating conditions, absorptive loads within the amplifier dissipate approximately 10 W of heat; under extreme conditions, this value may increase to 50 W, creating a critical thermal management challenge. Conventional ground-based cooling techniques, such as water or forced air cooling, cannot be applied in space. Consequently, heat dissipation relies exclusively on conduction and radiation through the satellite mounting plate and structural frame [58].

2.3. Filters

With the increasing density of satellites, the demand for spatial and spectral filtering has become more critical. Strong out-of-band signals may saturate wideband amplifiers or generate intermodulation products, thereby degrading communication quality. Filters are among the most indispensable components of satellite communications and electronic countermeasure systems. Their primary role is frequency selection, achieved through circuit structures and frequency-response characteristics that attenuate high-frequency noise and suppress low-frequency oscillations caused by power supply fluctuations [59]. In this way, filters effectively mitigate signal attenuation and interference. In recent years, growing requirements for bandwidth expansion have driven research worldwide towards the development of tunable high-performance filters (Figure 12). Such filters can dynamically adjust their center frequencies or bandwidths. Despite impressive advances, most proposed solutions still exhibit shortcomings in bandwidth performance and rely on experimental verification methods that require further refinement [60].

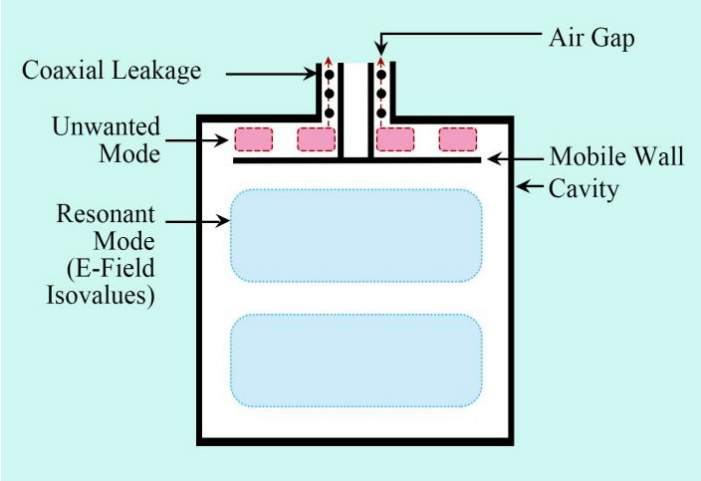


Figure 12. Tunable filter.

The increasing need for high-precision real-time processing in satellite communication has encouraged the integration of advanced algorithms with filters [61–63]. For instance, spectrum monitoring schemes based on dual-granularity recursive Bayesian inference [64] have been applied to user terminals for communication security. Kalman filtering, widely used in integrated navigation systems, has also been adapted for satellite communication. By recursively estimating current states from previous data and observations, Kalman filtering effectively suppresses noise and interference [65]. More recently, innovative frameworks integrating quantum neural networks into Kalman filtering have been proposed [66], which can significantly improve prediction accuracy, reduce mean absolute error, and enable scalability across various noise environments.

Technical research on spaceborne filters is advancing rapidly in line with the demands for higher-level communication systems and stricter requirements for frequency-response stability. Common problems include: (1) degradation of filter performance, which affects noise suppression; (2) abnormal frequency responses deviating from design values; (3) impedance mismatches at input or output, leading to reflection and signal loss; (4) increased bit error rates due to nonlinear group delay, in-band ripple, or out-of-band rejection deficiencies; and (5) thermal damage, component fatigue, and mechanical faults. Such issues often interact to form cascading chain failures, thereby amplifying the degree of malfunction. Ongoing research in several countries has made progress in addressing these issues. Virtual simulation technologies have been increasingly applied to reproduce

in-orbit conditions and develop targeted compensation strategies for filter models. This has provided valuable insights into filter failure mechanisms and guided improvements in the design, reliability, and transmission performance, thereby supporting the continued development of advanced spaceborne filters.

2.3.1. Signal Attenuation

Unlike power amplifiers and frequency converters, spaceborne filters are passive components that do not generate heat actively. Their performance degradation is typically manifested as increased insertion loss, passband frequency offset [67], and abnormal energy transfer caused by micro-discharge effects. Gradual failures induced by environmental thermal cycling often occur in dielectric materials and mechanical structures, with additional influencing factors including conductor material degradation, dielectric lattice radiation damage, and ohmic losses [68]. Micro-discharge effects are most prominent in resonator cavity regions, where a high Q-factor is maintained. In such cases, insufficient filtering may occur when the signal frequency is close to the filter cutoff range. Moreover, traditional signal enhancement techniques designed to suppress interference may inadvertently misclassify useful signals as noise, resulting in over-suppression [69], as illustrated in Figure 13. Consequently, useful signal energy is absorbed or lost, leading to gradual attenuation, a reduced signal-to-noise ratio [70], and a decline in overall communication quality. Although such losses do not directly damage the filter components, they severely impair system performance.

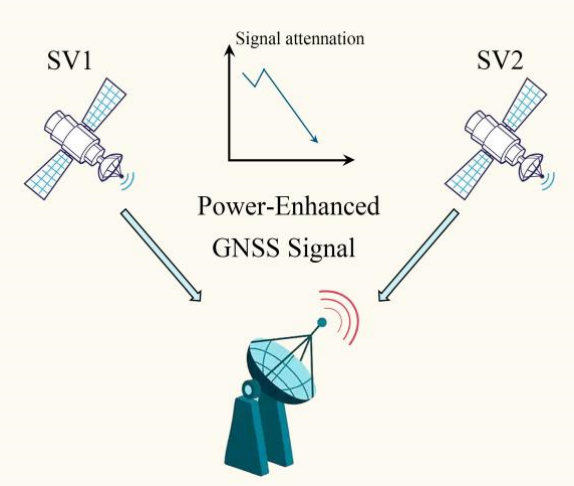


Figure 13. Signal boosting methods to suppress interference.

2.3.2. Abnormal Frequency Response

An abnormal frequency-response represents a fundamental failure mechanism responsible for significant performance degradation. This distortion originates from the nonideal frequency response characteristics of the filters and extreme environmental conditions. Under such influences, the transfer function $H(f)$ becomes distorted. Once the accumulated distortion exceeds a critical threshold, it directly impacts signal amplitude, phase, and time-domain waveform integrity [71]. When combined with Doppler frequency shifts, these distortions can lead to dual-level failures: (1) at the signal level, causing demodulation errors or broadband capacity reduction, and (2) at the spectrum level, degrading filtering performance and potentially resulting in complete signal interruption. Merello et al. [72] investigated Ku-band filters with varying substrate integration technologies under space vibration environments and observed changes in the natural frequency and electrical response, further confirming the susceptibility of filters to mechanical stress conditions.

2.3.3. Signal Reflection

In satellite communication systems, signal reflection (i.e., degradation of return loss) is a common failure mode in spaceborne filters. Unlike performance degradation, where signals are absorbed, signal reflection refers to the backward reflection of energy. This phenomenon is typically caused by impedance discontinuities (e.g., mismatches with transmission line impedance) or by radiation-induced deformation of cavity or dielectric structures, which shifts the center frequency. When reflected waves overlap with incident waves, standing waves are generated, significantly increasing the voltage standing wave ratio and thereby posing severe risks of failure [73]. Impedance mismatch is strongly influenced by environmental stresses such as temperature fluctuations and mechanical loading. At low temperatures, dielectric capacitance decreases sharply, whereas at high temperatures, electrolyte evaporation further shifts capacitance away from its design values. Similarly, magnetic core saturation in inductors reduces permeability, leading to lower inductance and consequently altering the input–output impedance. In orbit, high-frequency vibrations and microgravity conditions may cause microstrip line fractures or inductor displacement. Such failures disrupt electromagnetic field distribution, increase passband ripple, and exacerbate impedance deviation.

Although the mechanisms of signal loss and signal reflection differ, both may occur simultaneously or be causally linked in actual systems, and their severity levels vary. When impedance mismatch arises at the filter input port, the signal energy is divided into two parts: one is reflected, while the remainder is transmitted with reduced efficiency. Radiation damage further increases dielectric loss, increases insertion loss, and alters material properties, which aggravates reflection [74]. Therefore, studies on failure phenomena often associate signal reflections with signal loss. However, compared with loss, signal reflection poses greater risks because it may trigger cascading device-level failures, whereas loss primarily reduces link transmission quality [75].

2.3.4. Bit Error Rate Degradation

Power enhancement is a critical approach for strengthening the anti-interference capabilities of satellite communication systems. To accommodate such signals, multiplexer filters following the power amplifier are usually configured in multi-channel mode, thereby improving signal selectivity. However, owing to limitations in the design and fabrication, issues such as nonlinear group delay, in-band ripple, and insufficient out-of-band rejection frequently arise. The responses of such filters deviate from ideal linearity. Moreover, given the limited signal power margin and high operating frequency of the Ka-band widely employed in satellite communication, Doppler shifts caused by the high dynamics of LEO satellites remain a considerable challenge, making it difficult to completely suppress interference. Additionally, the rapid relative motion between LEO satellites and ground terminals introduces abrupt dynamic accelerations in the line-of-sight direction, which forces receivers to reduce coherent integration time and adapt to varying environmental conditions [76]. Under these circumstances, carrier frequency and code phase exhibit nonlinear time-varying characteristics, leading to carrier frequency offset. This results in frequency mismatches, in-band distortion, an increased demodulation bit error rate, and degraded filtering performance. Severe cases may cause loss of lock, thereby increasing the risk of system failure beyond terrestrial filter levels.

With the continuous advancement of LTE communication technologies, more stringent specifications for group delay variations have been introduced. For instance, the European DVB-S2X Digital Video Broadcasting Standard specifies a maximum group delay variation of 5 ns/MHz for spaceborne filters [77]. In comparison, 4G-LTE applications require variations not exceeding 0.5 ns/MHz. Therefore, research across multiple countries has

focused on developing miniaturized, high-performance filters that provide lower insertion loss, wider passband bandwidth, higher center frequency, and improved out-of-band rejection [78–80]. Excessive group delay variation in spaceborne filters not only causes in-band distortion and inter-symbol interference but also degrades error vector magnitude during receiver demodulation, ultimately resulting in higher system-level bit error rates.

Practical constraints, such as device size, weight, and operating conditions, further complicate filter design. Consequently, spaceborne filters often exhibit increased passband ripple and high stopband rejection [81]. To address these issues, Zhang et al. [82] proposed a new high-performance microwave photonic filter (MPF) based on vector compound-stimulated Brillouin scattering (SBS). The MPF overcame the inherent bandwidth limitations of natural SBS and demonstrated superior out-of-band rejection. In addition, a range of narrowband tunable filtering solutions has been developed, including fiber Bragg gratings [83]. Fabry–Perot cavities [84], high-birefringence fiber loop mirrors [85], Mach–Zehnder interferometers [86], and cascaded microring resonators [87,88]. Xu et al. [89] proposed an MPF with ultra-narrow bandwidth, wide tuning range, and high-frequency selectivity. The structure employed a Brillouin laser resonator composed of a 100 m primary cavity cascaded with a 10 m secondary cavity, enabling efficient ultra-narrowband filtering.

Reference [90] introduced a cascaded N-path filter architecture designed to improve out-of-band and harmonic rejection (HR). Operating within a tunable frequency range of 0.2–1.2 GHz, the filter achieved more than 32 dB suppression of second- and third-order harmonics, along with the maximum out-of-band rejection of 55 dB. Low-temperature co-fired ceramic (LTCC) technology has also been applied to GPS frequency bands, in which an L-band wide stopband filter was designed using an eight-layer LTCC dielectric. This design achieved a passband insertion loss as low as 1.6 dB, a return loss better than 30 dB, and stopband suppression up to 16 GHz [91]. In addition, filter-integrated low-noise amplifiers developed for Ku-band satellite communications [92,93] demonstrated high out-of-band rejection, while significantly improving flexibility and scalability in design.

At present, nonlinear effects caused by group delay fading in spaceborne filters remain unresolved. These effects introduce inter-symbol interference at the receiver, ultimately degrading the decoding performance of satellite communication systems. To address this, it is necessary to establish accurate models of the strong nonlinear characteristics of spaceborne filters and further investigate the in-orbit operational behavior of such devices, with the objective of improving their impact on satellite transmission systems.

2.4. Frequency Converter

The frequency conversion circuit of a spaceborne frequency converter consists of modulation, demodulation, and mixing units. The up-conversion and down-conversion correspond to upper mixing and lower mixing, respectively. The primary functions include up-converting and amplifying the analog downlink signal for transmission as well as down-converting the received RF signal from the simulator output to meet the frequency band requirements of satellite-to-ground or inter-satellite links [94].

As shown in Table 2, among the core components, the role of the LO source is to generate the LO signal required for modulation, demodulation, and mixing in both transmit and receive channels. Currently, LO sources are primarily implemented using oscillators, direct digital synthesizers (DDS), and phase-locked loop (PLL) technologies. A mixer is a nonlinear device that produces oscillation frequencies equal to integer linear combinations of the frequency components of two input oscillators or signals [95]. Mixing is accomplished by exploiting the nonlinear or time-varying properties of the device to multiply the LO signal by an RF or intermediate frequency (IF) signal. Various implementation methods exist for mixers, among which passive mixers based on mixing diodes have been widely adopted.

Owing to their advantages of wide bandwidth, high linearity, and strong resistance to radiation, diode-based passive mixers have become a mainstream solution. The current across the mixing diode is expressed as

$$i = I_0 + I_{IF}\sum_{n=1}^{\infty} \frac{\left(\frac{e}{nKT}\right)^n}{n!}[U_{IF}\sin(2\pi f_{IF}t) + U_{LO}\sin(2\pi f_{LO}t)]^n, \quad (8)$$

where I_0 is the saturation current of the mixing diode, U_{IF} is the amplitude of the IF signal, f_{IF} is the frequency of the IF signal, U_{LO} is the amplitude of the carrier signal, and f_{LO} is the frequency of the carrier signal.

Table 2. Spaceborne inverter core components.

Component	Function	Key Technical Index
Mixer	Frequency computation	Conversion loss
Local oscillator (LO)	Provides a stable reference frequency	Phase noise
Filter	Suppresses spurious signals and harmonics	Out-of-band rejection
Amplifier	Compensates for link loss	Noise figure
Frequency synthesizer	Generates a tunable LO signal	Frequency resolution

After the IF and LO signals enter the mixer, they are combined to produce an RF output frequency, which is expressed as

$$f_{RF} = f_{LO} \pm f_{IF}, \quad (9)$$

In some cases, active mixer transistors have been employed. Although they provide gain, their use requires strict evaluation in spaceborne systems, where high reliability is essential.

Based on conversion modes and architectures, spaceborne frequency converters can be classified into four categories: single conversion, superheterodyne (dual conversion), direct conversion, and microwave photonic conversion. Single conversion structures, as their name implies, can perform a single frequency conversion using a mixer and LO. They are simple in structure and low in cost, but are limited in handling wideband signals and achieving high image rejection. Consequently, they have been largely phased out. The superheterodyne structure employs two stages of frequency conversion, distributing filtering tasks across different intermediate frequencies. This reduces the performance requirements for individual filters, particularly for the first IF filter, which is less demanding than the RF filter used in a single conversion. This architecture offers superior selectivity, sensitivity, and stability, making it the most mature and widely applied structure in spaceborne systems. Nevertheless, it suffers from drawbacks such as increased circuit complexity, higher power consumption, and potential intermediate-frequency interference. Direct conversion is the simplest architecture. The RF signal is directly converted to or from the baseband without passing through an IF stage, thereby eliminating the need for expensive IF filters and associated processing. However, it faces significant challenges, including LO leakage, even-order harmonic distortion, and I/Q imbalance. Therefore, this approach is mainly adopted in applications that require low-power consumption and high miniaturization. Microwave photonic frequency conversion is a cutting-edge technology in which an RF signal is modulated onto an optical carrier. Conversion is then achieved using optical devices and optical signal processing. Given the diverse requirements of frequency converters and the frequent need for replacement or adaptation, additional solutions such

as frequency-division switching are considered in the design to support multiple frequency signal types.

Unlike other spaceborne electronic components, the primary functionality of spaceborne frequency converters is to maintain frequency purity. Accordingly, the main failure mechanisms are associated with frequency accuracy and phase stability, with most issues concentrated in the LO and mixing stages. Typical faults include unstable frequency conversion outputs and overshoot problems.

2.4.1. Unstable Frequency Conversion Output

When IF signals are up-converted to RF signals in the transmitter and subsequently down-converted back to IF in the receiver using mixers and LOs, output instability frequently arises during the conversion process. Ensuring frequency and phase lock is essential to mitigate power fading issues [96].

The harmonic architecture of frequency converters is highly susceptible to undesirable harmonics and pulse-width modulation [97], which lead to imbalance and saturation and cause fluctuations in output stability. To address these problems, high-performance filters are often required. However, this increases chip area, DC power consumption, and overall system complexity. Additional amplifiers are frequently inserted in the chain to compensate for multiplier losses, which can further exacerbate output instability [98]. Furthermore, as the harmonic order increases, subharmonic mixers suffer from higher conversion losses and degraded noise figures. In future designs, optical frequency comb technology may offer a potential solution by fundamentally eliminating electronic harmonic losses.

The direct interconnection between up-converters and down-converters may result in low output power, necessitating the utilization of an isolation amplifier as a "one-way valve" to prevent oscillation circuits from consuming useful signal power. In emerging technologies, microwave photonic mixers may also produce spurious mixing products at the output port, with sideband suppression ratios sometimes falling below safe thresholds. Although carrier-suppressed optical double sideband and carrier-suppressed optical single sideband methods [99] have been proposed to suppress such spurious signals, double-sideband modulation still faces power fading owing to optical fiber dispersion, which results in destructive interference [100].

2.4.2. LO Frequency Unlock

Phase-locked loops (PLLs) are widely employed control technologies for switching between frequency converters and power grids, particularly in high-frequency operations. PLLs stabilize the LO output frequency by locking the frequency or phase within a specified threshold. LO unlock occurs when the PLL fails to maintain the LO output frequency within the defined tolerance, typically manifested as frequency hopping or slow frequency drift on a spectrum analyzer, which results in severe reception interference and communication interruptions.

When the frequency deviation $\Delta f > \frac{f_{PD}}{2}$, the phase detector can no longer identify the phase difference, resulting in a complete loss of locking. In practice, extreme environmental conditions remain the dominant cause of PLL unlock. High-energy particles impacting PLL chips, such as frequency dividers or phase detectors, generate transient current pulses that abruptly alter the VCO tuning voltage. Cumulative radiation exposure further leads to junction capacitance drift in varactor diodes and dielectric degradation in the VCO resonator cavity. From a circuit design perspective, the loop filter is the most failure-prone component, in addition to natural aging effects over device lifetime. Loop bandwidth and phase margin are critical parameters that require precise control. If the bandwidth is excessively wide or narrow, stability is compromised. Typically, the maximum loop

bandwidth should not exceed one-tenth of the phase comparison frequency, whereas the minimum bandwidth must remain sufficient to ensure frequency stability of the controlled VCO. Phase margin corresponding to the damping factor in the time domain is another key determinant of stability. A larger phase margin improves damping, reduces oscillation amplitude, and enhances system stability, whereas a smaller margin increases oscillation and increases instability risks [101]. Empirical studies have suggested that a phase margin above 45° ensures stability, with 45–60° considered optimal. Nevertheless, task-specific communication requirements may require adjustments on a case-by-case basis. A rare unlock condition, termed cross-talk unlock, can also occur when two PLLs operate at identical or closely spaced frequencies. In such cases, mutual pulling between the VCO frequencies results in loss of lock.

Locking itself represents only the initial stage of PLL design. Persistent issues, such as phase noise and spurious signal generation, remain challenging and require further optimization. Consequently, PLLs with ultra-low phase noise, effective spurious and harmonic suppression, and enhanced radiation resistance are urgently required [102].

2.4.3. Overshoot Phenomenon

The overshoot phenomenon is distinct from yet causally related to the LO frequency unlock. It can be regarded as an "overreaction" of the control loop, potentially triggered by self-turn-on during shutdown [103], environmental radiation, or transient control imbalance resulting from loop response overshoot. Overshoot often serves as an early warning indicator of potential unlocking events. In contrast, the LO frequency unlock denotes the complete loss of steady-state synchronization [104]. When the PLL tracks frequency hops or attempts to suppress disturbances, an excessively high loop gain, insufficient phase margin, or damping-induced oscillation may produce overshoot failure. Such failures generally lead to localized disturbances within the communication system, including degradation of EVM or fluctuations in the power control loop, but do not initially threaten system stability. However, if unresolved, the overshoot may progressively intensify and ultimately evolve into an unlock, thereby aligning with the failure mechanisms discussed in the previous section.

2.5. Spaceborne Cable Assemblies

2.5.1. RF Connectors

Connectors are essential components that enable signal transmission, device interconnection, and passive intermodulation (PIM) control. They exist in numerous types and in large quantities and are widely applied in antenna systems. Common examples include SMA and N-type connectors.

In harsh space environments, connector failures typically manifest as mechanical damage and nonlinear effects, both of which are complex and difficult to diagnose. Mechanical damage represents a universal failure mode across electronic components, and nonlinear effects associated with connectors [105] have emerged as a major research focus. The PIM behavior of connectors is highly sensitive to environmental variations. During early assembly and initial operation, the system may perform with acceptable PIM levels. However, as time progresses, material degradation and contact performance deterioration may alter nonlinear characteristics, resulting in sudden PIM generation. These nonlinearities are generally categorized as material nonlinearity and contact nonlinearity.

Research on Passive Intermodulation in RF Connectors

Material nonlinearity arises from the intrinsic nonlinear conductive properties of materials, including ferromagnetic effects, electrostriction, and magnetoresistance. Contact nonlinearity refers to the nonlinear current and voltage behavior at metal contact points

within the connector. Such nonlinearities are induced by diverse contact interfaces, giving rise to PN junction-like effects such as quantum tunneling, thermionic emission, and Schottky conduction. Loose contact and rough contact surfaces further exacerbate these effects. Numerous domestic and international studies [106–109] have reported findings on PIM mechanisms.

Research on material nonlinearity has primarily focused on different metallic and magnetic substances, and considerable progress has been made. Bayrak et al. [110] conducted experimental studies on the intermodulation properties arising from contact between various metallic materials. Comparative experiments revealed that contacts such as copper–copper, brass–beryllium–copper, low-carbon steel–aluminum, and stainless steel generated strong intermodulation products, whereas surface coatings with gold, silver, rhodium, copper, or tin significantly reduced intermodulation levels. Ignea et al. [111] investigated distortion issues caused by ferromagnetic materials in GSM transmission and processing equipment. Using the Rayleigh model, they analyzed the two-tone response of ferromagnetic materials and validated the model through coaxial transmission line experiments. To mitigate PIM induced by material nonlinearity, ferromagnetic metals are generally avoided in practical applications. Common strategies include the use of brass and nickel–silver materials, whereas plating techniques typically exclude nickel coatings.

The contact state of RF connectors is inherently imperfect. Variations in the physical properties of contact surfaces caused by electrical and thermal effects, surface roughness, corrosion, and mechanical pressure can significantly alter connector performance. Vicente et al. [112] proposed a model to calculate the intermodulation power generated in rectangular waveguide connections, considering the roughness of metal–insulator–metal (MIM) contact surfaces and the presence of surface oxides. Their results indicated that the contact load between metals was a critical factor affecting PIM levels, where low contact pressure combined with high surface roughness led to strong intermodulation interference, whereas corrosion had little influence. At higher pressures, the effect of roughness diminished, and corrosion on the contact surface became the primary contributor to PIM [112]. Henrie et al. [113] reported the cancellation of PIM from multiple locations within a system by controlling gold and nickel plating thickness on coaxial connector conductors. Contact surface roughness was found to exert a significant influence [114]. According to Holm's electrical contact theory (Figure 14), any contact surface essentially consists of micro-protrusions, where current flow produces constriction resistance, and non-contact areas form capacitive effects. In engineering practice, strategies such as enlarging the contact area, reducing surface roughness, designing stable contact structures, and applying protective coatings against oxidation and corrosion are widely adopted to mitigate the nonlinear effects of contacts [115].

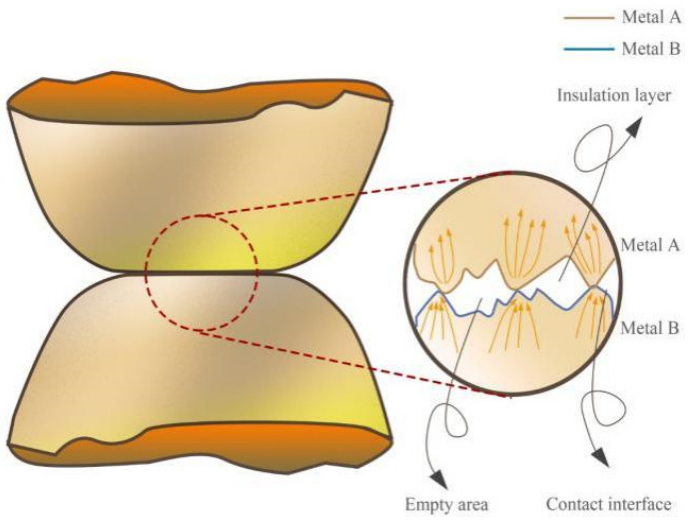


Figure 14. Microstructure of metal–to–metal contact surfaces.

Failure and Reliability Analysis of RF Connectors

The reliability of connectors is highly sensitive to environmental stress, mechanical structure, and contact conditions [116]. It is generally divided into design reliability and usage reliability, both of which are largely determined by environmental performance, mechanical performance, and electrical performance.

Common environmental performance indicators include temperature resistance, radiation resistance, corrosion resistance, vibration, and shock. Numerous test methods have been developed to evaluate the environmental impact of connectors. For RF connectors, mechanical performance is primarily characterized by the insertion and withdrawal force and the mechanical lifespan. Among these, insertion and withdrawal force can be the most critical parameters and a main cause of mechanical failure. It is influenced by the structural design of the connector (which determines the contact pressure), quality of the plating at the contact point (affecting sliding friction), and dimensional precision of alignment (affecting adjustment accuracy). These factors can lead to stress relaxation and fretting wear under alternating vibrations. Yang et al. [117] analyzed the PIM variation in loosened connectors and showed that poor connections increased current density in the contact area, thereby elevating PIM levels.

At higher operating frequencies, dust on contact surfaces or component relaxation can significantly degrade the electrical performance. In complex electromagnetic environments, conventional parameters such as contact resistance, insulation resistance, and dielectric withstand strength are no longer sufficient to fully evaluate electrical reliability. Instead, a comprehensive assessment should include high-frequency parameters and electromagnetic compatibility, such as return loss, insertion loss, voltage standing wave ratio, electromagnetic leakage, and power capacity. Connector reliability studies in this domain require strict standards and advanced testing protocols. Timsit et al. [118] investigated electrical performance under high-frequency conditions using finite element models and analyzed the effects of frequency on resistance, capacitance, and inductance at high-speed interfaces. Malucci et al. [119,120] further studied the microscopic impact of contact impedance on high-speed signals, deriving analytical models for multipoint contact surfaces. Their results provide valuable insights into frequency-dependent variations and the mechanisms underlying the degradation of high-frequency electrical reliability.

In summary, connectors are prone to degradation under extreme environments. Although research on reliability improvement has advanced, a significant gap remains be-

tween current achievements and the ideal state. Establishing more rigorous standards and comprehensive evaluation methods will be a major scientific challenge for future studies.

2.5.2. Cables

To satisfy diverse requirements for frequency range, insertion loss, and power handling, spaceborne cables are typically designed as shielded types, with external metallic shielding layers to suppress electromagnetic interference [121,122]. Based on their communication functions, space-grade cables are generally divided into three categories: power cables, data cables, and RF cables. Notably, data cables are the most fragile, whereas RF cables exhibit relatively high reliability. The cross-sectional diagrams of the three cable types are presented in Figure 15.

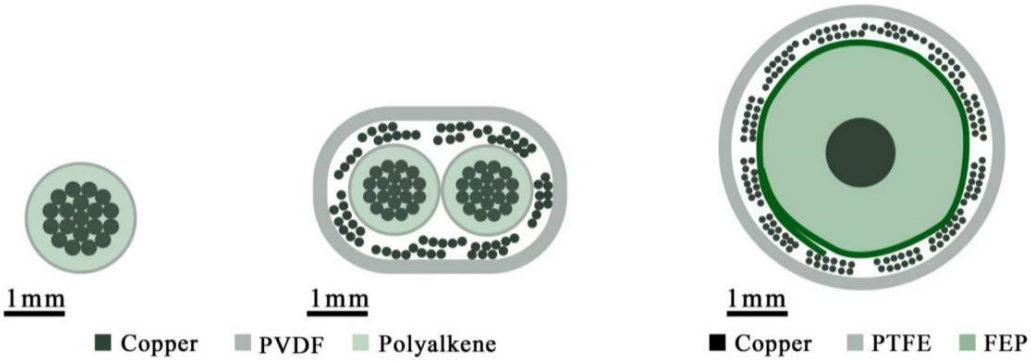


Figure 15. Cutaway view of power cable (**left**), data cable (**center**), and RF cable (**right**).

The failure analysis of cables requires comprehensive consideration of material selection, assembly processes, and operational maintenance. Mechanical failure is particularly frequent, arising from fatigue cracking of protective layers under vibration or frictional impact, as well as from poor or detached contact between inner and outer conductors. Because vibration-induced fatigue is inevitable, its mitigation relies on appropriate material selection, redundancy, and structural optimization. In cable-to-connector assemblies, poor inner conductor contact may result from mismatched pin dimensions, dimensional deviations at the cable–connector interface, or incomplete inner conductor soldering. Poor outer conductor contact may arise from gaps between the connector shell and sleeve or from insufficient soldering between the connector sleeve and cable shield. Detached inner or outer conductor contacts are generally attributed to improper assembly processes.

Reference [123] examined mechanical damage failure modes in spaceborne cables through hypervelocity impact (HVI) tests on various cable types [124]. The reliability was assessed under alternating shielding conditions formed by representative spacecraft structural walls. The observed failure modes included: (1) short circuits caused by melted or vaporized aluminum conductors and (2) strand bending due to impact debris, resulting in short circuits between the shield and signal cable. These findings indicate that most cable failures can be driven by mechanical damage and electrical interference, although the severity of these two factors cannot always be correlated directly.

In addition to mechanical failure, poor signal transmission quality may arise from low dielectric breakdown strength, arcing behavior, impedance mismatch, radiation damage, and space charge accumulation [125], all of which degrade the electrical performance of cables. Dielectric weakness and arcing are critical in high-power transmission or complex electromagnetic environments. Arc discharges form within the insulation when subjected to high voltages or strong electric fields, leading to circuit breakdown, short circuits, and carbonization of the insulation layer. To improve the understanding of such fault mechanisms, extensive international “arc tracking” tests have been conducted, focusing

on arc behavior and insulation materials [126]. The mechanism of impedance mismatch is similar to that observed in power amplifiers and other electronic components. Reflections at the interface produce standing waves, which cause signal attenuation, increase bit error rates, and reduce circuit lifespan. Radiation damage also plays a significant role, as thermal aging of conductors and insulation materials alters dielectric properties, reduces dielectric constant, and increases energy loss, ultimately causing signal attenuation and transmission delay. The application of new materials has been shown to effectively reduce such energy losses. Yu et al. [127] evaluated the feasibility of superconducting cables for spacecraft power transmission and proposed a design scheme based on HTS stacked tape round-core cables. These cables exhibit clear advantages in terms of high-power density and high efficiency. However, in vacuum environments, the insulation layer is prone to charge accumulation under high-energy particle radiation, leading to space charge regions that may discharge under specific conditions (Figure 16). Current research is focused on understanding space charge behavior in cables subjected to different thermal and electrical stresses [128]. This helps define the failure range associated with space charge accumulation [129], an area that has been widely investigated. Reference [130] further analyzed the influence of temperature gradients (TG) on charge accumulation, revealing that coaxial geometry and temperature gradients in the insulation layer intensify heterogeneous charge accumulation near the outer semiconducting layer of the cable.

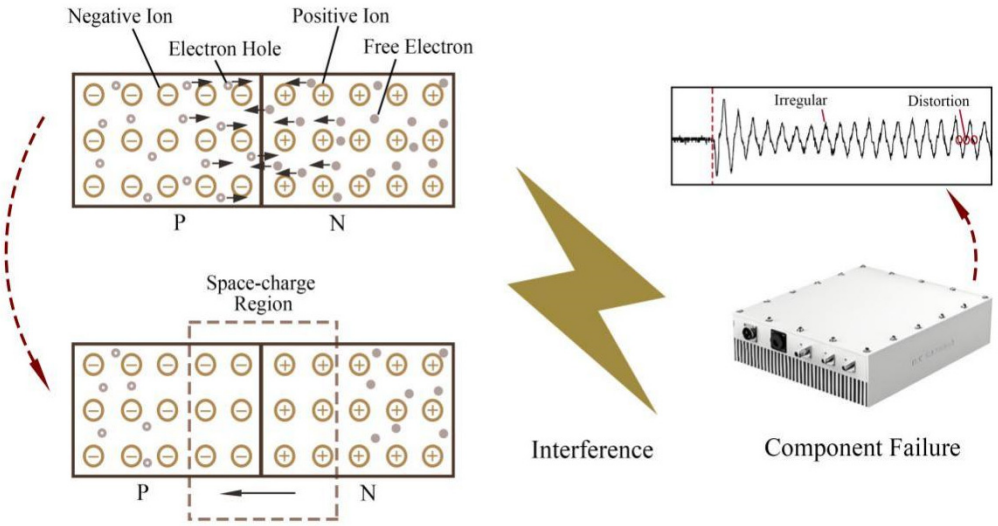


Figure 16. Space charge effect.

3. Development Trends

Based on the preceding research and discussions on the failure mechanisms of spaceborne electronic components, this section explores potential future development directions in on-orbit fault detection and repair technologies. The anticipated development trends for the fault detection and repair technologies of spaceborne electronic components are illustrated in Figure 17.

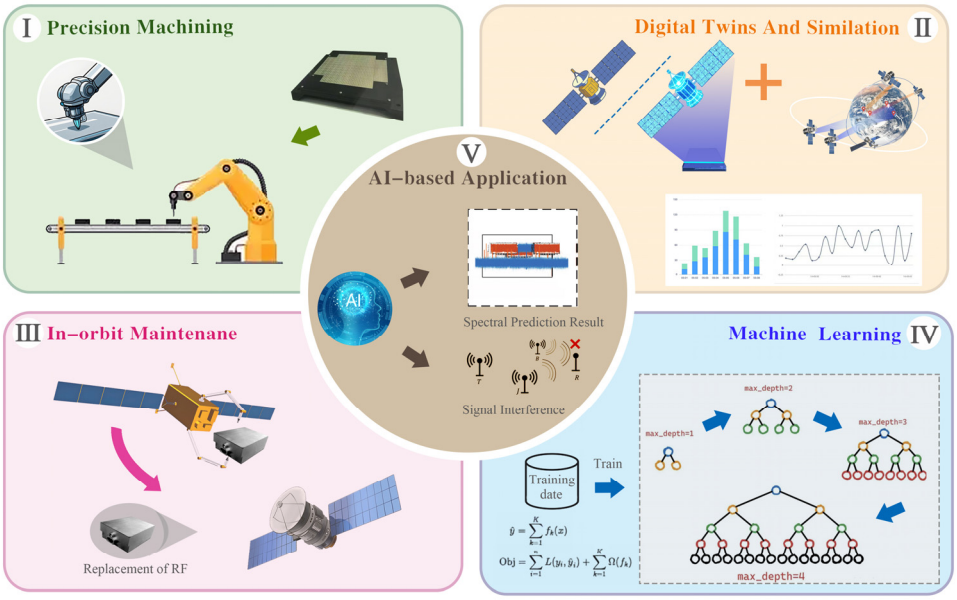


Figure 17. Future development trends of fault detection technology for spaceborne electronic components.

(1) Precision Machining: Spaceborne electronic components are highly susceptible to electrothermal effects, cracking, fatigue, and corrosion during long-term operation in extreme environments, which directly affects communication performance, reliability, and safety. Currently, global manufacturing technologies are advancing rapidly, with the United States, Germany, and Japan at the forefront. Precision machining has evolved from the "micron level" towards the "nanometer level". However, there remains significant potential for improvement in precision processing technologies as well as in the research and application of advanced composite materials. The future development trends in precision manufacturing technologies can be summarized as follows: (a) Additive Manufacturing (AM): Unlike conventional techniques such as welding and thermal spraying, additive manufacturing is an emerging repair method that offers high precision, complex shape reconstruction, and efficient material utilization. It is regarded as a promising solution for remanufacturing and customized design of electronic components. (b) High-Precision Assembly and Packaging: Traditional assembly and packaging methods are no longer sufficient to meet the demands of modern electronic devices, which require high performance, high integration, and miniaturization. High-precision assembly and packaging technologies adopt innovative design and manufacturing methods for integrated circuits, such as 3D packaging, fan-out wafer-level packaging (FOWLP), and embedded wafer-level ball grid arrays (eWLB), which represent highly promising directions. (c) Micro/Nano Manufacturing Technology: This area involves high-performance material design, processing, and manufacturing at micron (1 μm = 10^{-6} m) and nanometer (1 nm = 10^{-9} m) scales. These technologies are highly consistent with the manufacturing requirements for advanced spaceborne chips and other core components. (d) Ultra-Precision Machining: Techniques employing high-energy beams, such as laser beams, electron beams, and ion beams, have become increasingly mature and are widely applied in fine processing and surface modification of materials. Nevertheless, for complex structures and multi-material collaborative processing, challenges remain in achieving the desired precision, surface quality, and cost control. These issues are expected to be critical research directions in the future of aerospace manufacturing.

(2) On-orbit fault prediction based on digital twin and simulation technology: As illustrated in Figure 18, the satellite digital twin constructs a high-fidelity virtual model con-

sistent with the physical satellite, thereby enabling uninterrupted closed-loop interaction and data fusion between the satellite and its virtual counterpart. This facilitates real-time monitoring and assessment of satellite faults or damage. By combining physics-based and data-driven approaches, the concept of digital twins offers tremendous application potential for satellites, space stations, and other systems operating in orbit over the long term. Previous studies have used XGBoost classification models to verify that twin data closely mimics real satellite failure samples, with an average diagnostic accuracy of 98.8% for known failures. When combined with simulation technologies, it can realistically reproduce various on-orbit failure scenarios. Reference [131] proposed a digital-twin-based framework for detecting and protecting SH and GH nodes in satellite networks induced by SDC. The conventional approach relies on ground-based physical companion systems to perform load, environmental, and operational simulations identical to those of an actual mission, thereby reproducing the satellite's on-orbit state for inspection, maintenance, or replacement. However, this method is limited by constrained simulation capacity, high transportation costs, and low efficiency. Therefore, establishing a comprehensive digital satellite framework based on digital twin technology is of critical importance and represents one of the frontier directions in current satellite communication research.

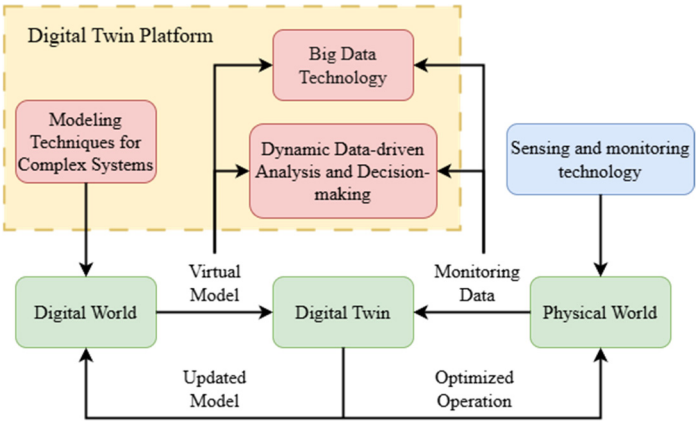


Figure 18. Key technologies for digital twins.

(3) Modular on-orbit manufacturing and maintenance: A key development trend in satellite communication is system integration and modular design, which promotes the standardization of interfaces and protocols, and the optimization of mechanical connection structures, thereby enabling plug-and-play functionality for components and modules. This approach is particularly advantageous in maintaining satellite communication systems in extreme environments. Communication electronic components are housed within detachable RF modules. Once a failure occurs or a component reaches the end of its service life, a robotic spacecraft for in-orbit services can simply replace the defective RF module using a robotic arm, a process comparable to replacing a car battery on Earth. This method can become an essential research focus for future on-orbit maintenance of communication systems.

(4) Data-driven machine learning models: Currently, machine learning methods are increasingly applied in satellite fault diagnosis and anomaly detection, such as Out-of-Distribution (OOD) analysis, XGBoost, Autoencoder, Deep Neural Networks (DNNs), and comparative learning. These models typically learn the distribution patterns of historical normal operational data, enabling anomaly identification, even without specific fault references. However, owing to the unique characteristics of satellite data, machine learning models face several challenges: (a) Model training depends heavily on historical fault data, which are extremely limited, and identified categories may not fully cover all failure

scenarios. (b) High requirements exist for both the quality and quantity of training datasets. (c) Models cannot reliably detect unknown or previously unseen faults, which may be misclassified as normal or other known faults, leading to missed or inaccurate diagnoses. Therefore, the application of machine learning models in satellite fault diagnosis remains at an early stage. To overcome this limitation, explicit physical constraints—such as the heat dissipation equations of power amplifiers, multipactor breakdown threshold conditions, and the frequency-response transfer functions of filters—can be embedded into the training and inference processes of data-driven models. Specifically, physics-informed neural networks (PINNs) and hybrid modeling strategies offer an effective implementation paradigm: they incorporate partial differential equations or empirical formulas that govern device failure mechanisms as regularization terms or constraints within the neural network loss function, compelling the model to comply with known physical laws while fitting the limited data. Through this joint physics–data-driven approach, the model is capable of producing physically consistent and reasonable predictions even in data-sparse regions, thereby constituting a key technical pathway for enhancing the reliability of spaceborne electronic devices.

(5) AI foundation models: AI research remains one of the most dynamic yet immature fields. Its initial applications included intelligent interference recognition and anti-jamming decision-making in extreme environments. In terms of interference detection accuracy, it outperforms traditional energy detectors by an average of about 30%. However, most current AI-related studies involve high implementation complexity and are not suitable for satellites. Algorithm optimization and complexity reduction are crucial directions for future research. Existing models primarily consider Gaussian white-noise channels, with little attention given to non-human interference sources, such as adjacent satellites, cosmic radiation, and solar wind. Future studies should comprehensively account for these extreme environmental factors. The application of AI in spectrum prediction is becoming increasingly widespread, significantly improving spectrum utilization. Research is expected to focus more on large-scale MIMO systems, with a particular emphasis on multi-node cooperative prediction in AI-assisted communication networks to enhance prediction accuracy as an emerging area of major interest. Additionally, AI-based data augmentation can be fully exploited to achieve faster and more accurate satellite fault forecasting with reduced data requirements. This approach complements machine learning-based fault detection techniques and represents a highly promising research direction.

4. Conclusions

For satellites facing communication failures or reaching the end of their operational life, effective health monitoring and fault management of spaceborne RF electronic components are critical challenges that require urgent solutions. This review focuses on in-orbit failures of satellite electronic components by systematically examining the developmental background and current applications of satellite communication technology. It analyzes potential factors affecting spaceborne RF modules in extreme space environments, including intense radiation, severe vibration, high vacuum, resource scarcity, and extreme temperatures. Detailed progress in research and failure mechanisms are presented for four core RF components: power amplifiers, filters, frequency converters, and RF assemblies. Potential failure phenomena are categorized according to both shared and component-specific mechanisms in ultra-compact RF modules. This encompasses shared triggers such as mechanical damage, electronic effects, and electromagnetic interference, along with distinct failure phenomena rooted in electronic component characteristics such as nonlinear distortion, incorrect power amplifier bias positioning, and abnormal frequency responses. This work lays a solid foundation for subsequent reliability technology research. Furthermore, this

review further outlines key bottlenecks in current reliability technologies and explores future research directions. It emphasizes the transformative potential of integrating five frontier technologies, including precision machining, digital twin and simulation, modular in-orbit manufacturing and maintenance, data-driven machine learning models, and AI, with satellite communication systems. Such integration is expected to drive continuous improvements in the reliability of satellite communications across both commercial and military domains.

Author Contributions: Writing—review and editing, visualization, writing—original draft, validation, S.Y.; writing—review and editing, conceptualization, H.W.; writing—review and editing, visualization, resources, project administration, funding acquisition, formal analysis, J.D. All authors have read and agreed to the published version of the manuscript.

Funding: Authors would like to thank the support by National Natural Science Foundation of China (Grant No. 52375004).

Conflicts of Interest: The authors declare that they have no known competing financial interests or personal relationships that could have appeared to influence the work reported in this paper.

References

1. You, L.; Li, K.X.; Wang, J.; Gao, X.; Xia, X.G.; Ottersten, B. Massive MIMO transmission for LEO satellite communications. *IEEE J. Sel. Areas Commun.* **2020**, *38*, 1851–1865. [CrossRef]
2. De Sanctis, M.; Cianca, E.; Araniti, G.; Bisio, I.; Prasad, R. Satellite communications supporting internet of remote things. *IEEE Internet Things J.* **2016**, *3*, 113–123. [CrossRef]
3. Kodheli, O.; Lagunas, E.; Maturo, N.; Sharma, S.K.; Shankar, B.; Mendoza Montoya, J.F.; Merlano Duncan, J.C.; Spano, D.; Chatzinotas, S.; Kisseleff, S. Satellite communications in the new space era: A survey and future challenges. *IEEE Commun. Surv. Tutor.* **2021**, *23*, 70–109. [CrossRef]
4. He, X.; Xu, C.; Tang, S.; Huang, Y.; Qi, W.; Xiao, Z. Performance analysis of an aerial remote sensing platform based on real-time satellite communication and its application in natural disaster emergency response. *Remote Sens.* **2024**, *16*, 2866. [CrossRef]
5. Yüceer, M. Emerging technologies for communication satellite payloads. *Prog. Aerosp. Sci.* **2012**, *50*, 27–34. [CrossRef]
6. Campajola, L.; Di Capua, F. Applications of accelerators and radiation sources in the field of space research and industry. In *Applications of Radiation Chemistry in the Fields of Industry, Biotechnology and Environment*; Venturi, M., D'Angelantonio, M., Eds.; Springer: Cham, Switzerland, 2016; pp. 269–297.
7. Li, X.Y.; Jian, Y.B.; Guo, Z.Y.; Sun, N.G.; Zhang, J.C.; Wang, J. System design and verification of high-speed camera system under extreme cryogenic and vacuum environment. In *Proceedings of the2017 International Conference on Optical Instruments and Technology: Advanced Optical Sensors and Applications, Beijing, China, 28–30, October 2018*; Zhang, X.P., Xiao, H., Arregui, F.J., Dong, L.Q., Eds.; SPIE: Bellingham, WA, USA, 2018.
8. Eswarappa Prameela, S.; Pollock, T.M.; Raabe, D.; André Meyers, M.; Aitkaliyeva, A.; Chintersingh, K.; Cordero, Z.C.; Graham-Brady, L. Materials for extreme environments. *Nat. Rev. Mater.* **2023**, *8*, 81–88. [CrossRef]
9. Guan, Q.; Hang, C.; Li, S.; Yu, D.; Ding, Y.; Wang, X.; Tian, Y. Research progress on the solder joint reliability of electronics using in deep space exploration. *Chin. J. Mech. Eng.* **2023**, *36*, 22. [CrossRef]
10. Al-Hraishawi, H.; Chougrani, H.; Kisseleff, S.; Lagunas, E.; Chatzinotas, S. A survey on nongeostationary satellite systems: The communication perspective. *IEEE Commun. Surv. Tutor.* **2023**, *25*, 101–132. [CrossRef]
11. Su, Y.; Liu, Y.; Zhou, Y.; Yuan, J.; Cao, H.; Shi, J. Broadband LEO satellite communications: Architectures and key technologie. *IEEE Wirel. Commun.* **2019**, *26*, 55–61. [CrossRef]
12. Agnesi, C.; Vedovato, F.; Schiavon, M.; Dequal, D.; Calderaro, L.; Tomasin, M.; Marangon, D.G.; Stanco, A.; Luceri, V.; Bianco, G.; et al. Exploring the boundaries of quantum mechanics: Advances in satellite quantum communications. *Philos. Trans. R. Soc. A Math. Phys. Eng. Sci.* **2018**, *376*, 20170461. [CrossRef]
13. Sodagari, S. Integrating quantum and satellites: A new era of connectivity. *IEEE Access* **2023**, *11*, 145101–145110. [CrossRef]
14. Arapoglou, P.D.; Liolis, K.; Bertinelli, M.; Panagopoulos, A.; Cottis, P.; De Gaudenzi, R. MIMO over satellite: A review. *IEEE Commun. Surv. Tutor.* **2011**, *13*, 27–51. [CrossRef]
15. Lu, K.; Liu, H.; Zeng, L.; Wang, J.; Zhang, Z.; An, J. Applications and prospects of artificial intelligence in covert satellite communication: A review. *Sci. China Inf. Sci.* **2023**, *66*, 121301. [CrossRef]
16. Luo, J.; Feng, J.; Gong, Y. A review of microwave vacuum devices in China: Theory and device development including high-power klystrons, spaceborne TWTs, and Gyro-TWTs. *IEEE Microw. Mag.* **2021**, *22*, 18–33. [CrossRef]

17. Lafontan, X.; Kuchenbecker, J.; Guillon, B.; Pons, P.; Nerin, P.; Pressecq, F.; Dardalhon, M.; Rigo, S. Mechanical qualification of RF-filters for space applications. In *Proceedings of the Symposium on Design, Test, Integration and Packaging of MEMS/MOEMS 2003, Washington, DC, USA, 30 April 2003*; IEEE: Piscataway, NJ, USA, 2003.
18. Briskman, R.D.; Kaliski, M.A.R. Transmitter microdischarges in communications and broadcast satellites. *Acta Astronaut.* **2016**, *126*, 163–167. [CrossRef]
19. Zhao, Y.; Sun, X.; Hu, T.; Bai, H.; He, Y.; Yang, J.; Cui, W.; Hu, Z.; Liu, M. Significantly reduced secondary electron emission from silver/carbon composite films for microwave devices. *J. Appl. Phys.* **2022**, *131*, 225301. [CrossRef]
20. Cao, G.M.; Wang, Z.Q. Multipactor in microwave system in space. *J. Astronaueic Metro. Meas.* **2002**, *5*, 1–5+12. (In Chinese)
21. Feng, H.; Liang, X.; Sun, J.; Feng, J.; Wei, Y.; Zhang, T.; Pu, X.; Zhang, D.; Xiang, Y.; Li, Y.; et al. Total ionizing dose effects of ^{60}Co-γ ray radiation on SiC MOSFETs with different gate oxide thickness. *Radiat. Eff. Defects Solids* **2023**, *178*, 1201–1210. [CrossRef]
22. Zhang, Z.; Guo, G.; Wang, L.; Xiao, S.; Chen, Q.; Gao, L.; Wang, C.; Li, F.; Zhang, F.; Zhao, S.; et al. Synergistic effects of total ionizing dose and single-event upset in 130 nm 7T silicon-on-insulator static random access memory. *Electronics* **2024**, *13*, 2997. [CrossRef]
23. Bezerra, F.; Ruffenach, M.; Ecoffet, R.; Carron, J.; Mekki, J.; Coïc, L.; Guillermin, J. 14 years of In-flight experimental data on CARMEN-MEX. *IEEE Trans. Nucl. Sci.* **2023**, *70*, 1533–1540. [CrossRef]
24. Lee, M. Complex design of CMOS logic with tolerance to particle and cumulative radiation. *IEEE Trans. Electron Devices* **2024**, *71*, 440–447. [CrossRef]
25. O'Bryan, M.V.; Wilcox, E.P.; Carstens, T.A.; Ryder, K.L.; Barth, J.D.; Osheroff, J.M.; Ryder, L.D.; Casey, M.C.; Joplin, M.B.; Lauenstein, J.; et al. NASA goddard space flight center's current radiation effects test results. In *2023 IEEE Radiation Effects DATA Workshop*; IEEE: Piscataway, NJ, USA, 2023.
26. Li, X.Y.; Sun, R.F.; Wang, Y.D. A review of typical thermal fatigue failure models for solder joints of electronic components. *2017 IOP Conf. Ser. Mater. Sci. Eng.* **2017**, *242*, 12103. [CrossRef]
27. Idumah, C.I. Thermal expansivity of polymer nanocomposites and applications. *Polym. Plast. Technol. Mater.* **2023**, *62*, 1178–1203. [CrossRef]
28. Casavola, C.; Pappalettera, G. Strain field analysis in electronic components by ESPI: Bad thermal contact and damage evaluation. *J. Nondestruct. Eval.* **2018**, *37*, 11. [CrossRef]
29. Cai, M.; Cui, P.; Qin, Y.; Geng, D.; Wei, Q.; Wang, X.; Yang, D.; Zhang, G. Entropy generation methodology for defect analysis of electronic and mechanical components-a review. *Entropy* **2020**, *22*, 254. [CrossRef]
30. Wang, M.; Lu, X.C.; Rao, Y.N. GNSS signal distortion estimation: A comparative analysis of L5 signal from GPS II and GPS III. *Appl. Sci.* **2022**, *12*, 3791. [CrossRef]
31. Rahman, M.M.; Kamruzzaman, M.; Shahid, S.; Thorp, K.R.; Rahaman, H.; Shahriyar, M.; Islam, A.K.M.S.; Huda, D. A GIS Framework to Demarcate Suitable Lands for Combine Harvesters Using Satellite DEM and Physical Properties of Soil. *J. Geovis. Spat. Anal.* **2023**, *7*, 27. [CrossRef]
32. Wang, Z.; Hu, S.; Gu, L.; Lin, L. Review of Ka-band power amplifier. *Electronics* **2022**, *11*, 942. [CrossRef]
33. Gunnarsson, S.E.; Karnfelt, C.; Zirath, H.; Kozhuharov, R.; Kuylenstierna, D.; Alping, A.; Fager, C. Highly integrated 60 GHz transmitter and receiver MMICs in a GaAs pHEMT technology. *IEEE J. Solid-State Circuits* **2005**, *40*, 2174–2186. [CrossRef]
34. Shinohara, K.; Regan, D.C.; Tang, Y.; Corrion, A.L.; Brown, D.F.; Wong, J.C.; Robinson, J.F.; Fung, H.H.; Schmitz, A.; Oh, T.C.; et al. Scaling of GaN HEMTs and schottky diodes for submillimeter-Wave MMIC applications. *IEEE Trans. Electron Devices* **2013**, *60*, 2982–2996. [CrossRef]
35. Hamada, H.; Tsutsumi, T.; Matsuzaki, H.; Sugiyama, H.; Nosaka, H. 475-GHz 20-dB-Gain InP-HEMT power amplifier using neutralized common-source architecture. In *Proceedings of the 2020 IEEE/MTT-S International Microwave Symposium (IMS), Virtual, 4–6 August 2020*; IEEE: Piscataway, NJ, USA, 2015.
36. Iwai, H. Future of nano CMOS technology. *Solid State Electron.* **2015**, *112*, 56–67. [CrossRef]
37. Chevalier, P.; Liebl, W.; Rücker, H.; Gauthier, A.; Manger, D.; Heinemann, B.; Avenier, G.; BÖck, J. SiGe BiCMOS current status and future trends in Europe. In *Proceedings of the 2018 IEEE BiCMOS and Compound Semiconductor Integrated Circuits and Technology Symposium (BCICTS), San Diego, CA, USA, 14–17 October 2018*; IEEE: Piscataway, NJ, USA, 2018.
38. Harame, D.L.; Ahlgren, D.C.; Coolbaugh, D.D.; Dunn, J.S.; Freeman, G.G.; Gillis, J.D.; Groves, R.A.; Joseph, A.J.; Subbanna, S.; Victor, A.M.; et al. Current status and future trends of SiGe BiCMOS technology. *IEEE Trans. Electron Devices* **2001**, *48*, 2575–2594. [CrossRef]
39. Flandre, D.; Raskin, J.P.; Vanhoenacker-Janvier, D. SOI CMOS transistors for RF and microwave applications. *Int. J. High Speed Electron. Syst.* **2001**, *11*, 1159–1248. [CrossRef]
40. Ma, K.X.; Mou, S.X.; Yeo, K.S. A study of CMOS SOI for RF, microwave and millimeter wave applications. In *Proceedings of the 2015 International Soc Design Conference (ISOCC), Gyeongju, Republic of Korea, 2–5 November 2015*; IEEE: Piscataway, NJ, USA, 2015.
41. Liou, J.J.; Schwierz, F. RF MOSFET: Recent advances and future trends. In *Proceedings of the 2003 IEEE Conference on Electron Devices and Solid-State Circuits (IEEE Cat. No.03TH8668), Hong Kong, China, 16–18 December 2003*; IEEE: Piscataway, NJ, USA, 2003.

42. Lang, D.V.; Logan, R.A.; Jaros, M. Trapping characteristics and a donor-complex (DX) model for the persistent-photoconductivity trapping center in Te-doped AlxGa1−xAs. *Phys. Rev. B* **1979**, *19*, 1015–1030. [CrossRef]
43. Shi, W.; Li, X.; Gao, Y.; Hu, C.; Dai, Z.; Pang, J.; Li, M. Load mismatch compensation of doherty power amplifier using dual-input and mode reconfiguration techniques. *IEEE Trans. Circuits Syst. I Regul. Pap.* **2023**, *70*, 2774–2787. [CrossRef]
44. Zhang, Z.; Fusco, V.; Cheng, Z.; Buchanan, N.; Guquad-band, C. A quad-band power amplifier based on impedance frequency modulation. *IEEE Trans. Circuits Syst. II Express Briefs* **2022**, *69*, 724–728. [CrossRef]
45. Jaraut, P.; Helaoui, M.; Chen, W.; Boulejfen, N.; Rawat, M.; Ghannouchi, F.M. Linearization of load mismatched power amplifiers using reflection-aware augmented polynomial model. *IEEE Trans. Circuits Syst. II Express Briefs* **2024**, *71*, 4025–4029. [CrossRef]
46. Aikio, J.P.; Rahkonen, T. A comprehensive analysis of AM–AM and AM–PM conversion in an LDMOS RF power amplifier. *IEEE Trans. Microw. Theory Tech.* **2009**, *57*, 262–270. [CrossRef]
47. Sharma, R.; Chaudhary, A.R.; Mehta, R.; Tomar, R.S.; Ozsahin, D.U.; Askar, S.; Ahmad, H. Power characteristics of a high-performance helix traveling wave tube. *Case Stud. Therm. Eng.* **2024**, *56*, 104199. [CrossRef]
48. Feng, W.; Wu, W.; Zhou, X.Y.; Che, W.; Shi, Y. Broadband high-efficiency quasi-class-J power amplifier based on nonlinear output capacitance effect. *IEEE Trans. Circuits Syst. II Express Briefs* **2022**, *69*, 2091–2095. [CrossRef]
49. Pelusi, M.; Kurosu, T.; Namiki, S. Power optimized brillouin amplifier for polarization independent low distortion gain. *Opt. Commun.* **2025**, *577*, 131420. [CrossRef]
50. Cha, J.; Yang, Y.; Shin, B.; Kim, B. An adaptive bias controlled power amplifier with a load-modulated combining scheme for high efficiency and linearity. In *Proceedings of the IEEE MTT-S International Microwave Symposium Digest, Philadelphia, PA, USA, 8–13 June 2003*; IEEE: Piscataway, NJ, USA, 2003.
51. Hau, G.; Nishimura, T.B.; Iwata, N. A highly efficient linearized wide-band CDMA handset power amplifier based on predistortion under various bias conditions. *IEEE Trans. Microw. Theory Tech.* **2001**, *49*, 1194–1201. [CrossRef]
52. Forestier, S.; Bouysse, P.; Quere, R.; Mallet, A.; Nebus, J.M.; Lapierre, L. Joint optimization of the power-added efficiency and the error-vector measurement of 20-GHz pHEMT amplifier through a new dynamic bias-control method. *IEEE Trans. Microw. Theory Tech.* **2004**, *52*, 1132–1141. [CrossRef]
53. Weiss, M.D.; Raab, F.H.; Popovic, Z. Linearity of X-band class-F power amplifiers in high-efficiency transmitters. *IEEE Trans. Microw. Theory Tech.* **2001**, *49*, 1174–1179. [CrossRef]
54. Ranjan, M.; Koo, K.H.; Hanington, G.; Fallesen, C.; Asbeck, P. Microwave power amplifiers with digitally-controlled power supply voltage for high efficiency and high linearity. In *Proceedings of the 2000 IEEE MTT-S International Microwave Symposium Digest (Cat. No.00CH37017), Boston, MA, USA, 11–16 June 2000*; IEEE: Piscataway, NJ, USA, 2000.
55. Yan, X.; Wang, P.; Wang, A.; Liu, W.; Hou, X.; Liu, J.; Ye, N. Unified constellation design using projection over QAM: Concept and examples. *IEEE Open J. Commun. Soc.* **2023**, *4*, 2343–2356. [CrossRef]
56. Ma, J.; Jindal, G.; Nair, M.; Cappello, T.; Watkins, G.; Morris, K.; Beach, M. Highly efficient 3-bit digital power amplifier for OFDM waveform amplification. *IEEE Trans. Microw. Theory Tech.* **2023**, *71*, 35–47. [CrossRef]
57. Liu, X.; Zhai, J.; Zhang, Z.; Ning, D.; Chen, P.; Yu, C. High-precision digital predistortion for sub-6-GHz GaN power amplifiers excited by a signal with 400-MHz modulation bandwidth. *IEEE Microw. Wirel. Technol. Lett.* **2024**, *34*, 552–555. [CrossRef]
58. Mistry, C.; Ghosh, S.K. Thermal design and analysis of radiation shield cooling assembly for efficient heat dissipation of space traveling-wave tube. *IEEE Trans. Electron Devices* **2024**, *71*, 374–380. [CrossRef]
59. Soares, E.R.; Fuller, J.D.; Morozick, P.J.; Alvarez, R.L. Applications of high-temperature-superconducting filters and cryo-electronics for satellite communication. *IEEE Trans. Microw. Theory Tech.* **2000**, *48*, 1190–1198. [CrossRef]
60. Laplanche, E.; Delhote, N.; Perigaud, A.; Tantot, O.; Verdeyme, S.; Bila, S.; Pacaud, D.; Carpentier, L. Tunable filtering devices in satellite payloads: A review of recent advanced fabrication technologies and designs of tunable cavity filters and multiplexers using mechanical actuation. *IEEE Microw. Mag.* **2020**, *21*, 69–83. [CrossRef]
61. Xiao, Y.; Zhou, X.; Wang, J.; He, Z.; Zhou, H. Observability analysis and navigation filter optimization of high-orbit satellite navigation system based on GNSS. *Appl. Sci.* **2020**, *10*, 7513. [CrossRef]
62. Murata, M.; Kawano, I.; Inoue, K. Degenerate gaussian sum filter for onboard satellite navigation and satellite reentry. In Proceedings of the AIAA Scitech 2021 Forum, Navigation, Estimation, Sensing, and Tracking III, Virtual, 11–15, 19–21 January 2021.
63. Khalife, J.; Neinavaie, M.; Kassas, Z.M. The first carrier phase tracking and positioning results with starlink LEO satellite signals. *IEEE Trans. Aerosp. Electron. Syst.* **2022**, *58*, 1487–1491. [CrossRef]
64. Ruan, T.; Huang, Y.; Wu, Q.; Quek, T.Q.S. Dual-grained recursive bayesian filtering for UAV-enabled satellite user terminal surveillance. *IEEE Trans. Veh. Technol.* **2025**, *74*, 8291–8296. [CrossRef]
65. Zhuang, Y.; Sun, X.; Li, Y.; Huai, J.; Hua, L.; Yang, X.; Cao, X.; Zhang, P.; Cao, Y.; Qi, L.; et al. Multi-sensor integrated navigation/positioning systems using data fusion: From analytics-based to learning-based approaches. *Inf. Fusion* **2023**, *95*, 62–90. [CrossRef]

66. Prakash, S.; Bhattacherjee, R.; Bitragunta, S.; Bhatia, A.; Tiwari, K. Quantum computing-accelerated kalman filtering for satellite clusters: Algorithms and comparative analysis. *IEEE Open J. Comput. Soc.* **2025**, *6*, 307–316. [CrossRef]
67. Jin, D.H.; Kim, J.H. Research on 5G signal interference removal device for satellite communication in C-band. *J. Korea Inst. Inf. Commun. Eng.* **2024**, *28*, 350–355.
68. Kahng, S.; Cho, J.; Seo, Y.; Lee, Y.; Jang, J.; Lee, H. Quality of satellite communication signals related to problems in RF components as hardware. In *Proceedings of the 2022 27th Asia Pacific Conference on Communications (APCC), Jeju Island, Republic of Korea, 19–21 October 2022*; IEEE: Piscataway, NJ, USA, 2022.
69. Song, J.; Lu, Z.; Xiao, W.; Li, C.; Wang, Y.; Sun, G. Power-enhanced GNSS interference mitigation with sensed equivalent bandwidth based on ASF algorithm. *IEEE Sens. J.* **2025**, *25*, 2886–2896. [CrossRef]
70. Won, J.H.; Eissfeller, B. A tuning method based on signal-to-noise power ratio for adaptive PLL and its relationship with equivalent noise bandwidth. *IEEE Commun. Lett.* **2013**, *17*, 393–396. [CrossRef]
71. Zhang, J.L.; Rao, Y.N. BDS-3 B2 frequency distortion signal generation. In *Proceedings of the 2024 9th International Conference on Electronic Technology and Information Science (ICETIS), Hangzhou, China, 17–19 May 2024*; IEEE: Piscataway, NJ, USA, 2024.
72. Merello, J.M.; Bachiller, C.; Nova, V.; Esteban, H.; Belenguer, Á. Study of vibration effects on communication filters in substrate integrated technologies. *IEEE Access* **2022**, *10*, 50418–50426. [CrossRef]
73. Savin, A.A. Analyzer of the GNSS simulators parameters. In *2014 IEEE Metrology for Aerospace (MetroAeroSpace)*; IEEE: Piscataway, NJ, USA, 2014.
74. Fisher, A.; Sinanis, M.D.; Khater, M.A.; Peroulis, D. EVAding interference: A hybrid architecture approach for substrate-integrated evanescent-mode cavity filters. *IEEE Microw. Mag.* **2023**, *24*, 61–67. [CrossRef]
75. Dakic, K.; Al Homssi, B.; Walia, S.; Al-Hourani, A. Spiking neural networks for detecting satellite internet of things signals. *IEEE Trans. Aerosp. Electron. Syst.* **2024**, *60*, 1224–1238. [CrossRef]
76. Iannucci, P.A.; Humphreys, T.E. Economical fused LEO GNSS. In *Proceedings of the 2020 IEEE/ION Position, Location and Navigation Symposium (PLANS), Portland, OR, USA, 20–23 April 2020*; IEEE: Piscataway, NJ, USA, 2020; pp. 426–443.
77. Ginesi, A.; Cioni, S.; Angelone, M. DVB-S2X channel models: Rationale and justifications. In *Proceedings of the 2014 7th Advanced Satellite Multimedia Systems Conference and the 13th Signal Processing for Space Communications Workshop (ASMS/SPSC), Vienna, Austria, 13 July 2014*; IEEE: Piscataway, NJ, USA, 2014.
78. Mohammadi, N.; Moloudian, G.; Roshani, S.; Roshani, S.; Parandin, F.; Lalbakhsh, A. A wilkinson power divider with harmonic suppression through low-pass filter for GSM and LTE applications. *Sci. Rep.* **2024**, *14*, 2429. [CrossRef]
79. Basit, A.; Daraz, A.; Zhang, G. Implementation of a wideband microwave filter design with dual electromagnetic interference (EMI) mitigation for modern wireless communication systems with low insertion loss and high selectivity. *Micromachines* **2003**, *14*, 1986. [CrossRef]
80. Udhayasuriyan, S.; Subramaniyan, S.; Johnson, W. A compact metamaterial-based open-ended CPW band-pass filter for wireless applications. *Arab. J. Sci. Eng.* **2022**, *47*, 3473–3480. [CrossRef]
81. Stefański, R.; Osiecki, A.; Stępień, J. Miniaturized S-band diplexers for space applications with high far out-of-band rejection. In *Proceedings of the 2024 25th International Microwave and Radar Conference (MIKON), Wrocław, Poland, 1–4 July 2024*; IEEE: Piscataway, NJ, USA, 2024.
82. Zhang, R.; Wang, W.; Li, M.; Zhu, N. Tunable microwave photonic filter with ultra-narrow passband and high out-of-band rejection. *J. Light. Technol.* **2024**, *42*, 7670–7677. [CrossRef]
83. Sano, Y.; Kobayashi, M.; Yoshino, T. Sideband-suppressed narrow bandpass fibre fabry-perot filter composed of fibre bragg grating and dielectric mirror. *Electron. Lett.* **2013**, *49*, 1350–1351. [CrossRef]
84. Pfeifer, H.; Ratschbacher, L.; Gallego, J.; Saavedra, C.; Faßbender, A.; von Haaren, A.; Alt, W.; Hofferberth, S.; Köhl, M.; Linden, S.; et al. Achievements and perspectives of optical fiber fabry-perot cavities. *Appl. Phys. B* **2022**, *128*, 29. [CrossRef]
85. Feng, X.; Tao, R.; Cao, Y.; Li, Z.; Guan, B. Complex coefficient microwave photonic filter based on multiwavelength phase modulation and PM-to-AM conversion. *Opt. Laser Technol.* **2013**, *45*, 110–113. [CrossRef]
86. Liu, X.; Yu, Y.; Tang, H.; Xu, L.; Dong, J.; Zhang, X. Silicon-on-insulator-based microwave photonic filter with narrowband and ultrahigh peak rejection. *Opt. Lett.* **2018**, *43*, 1359–1362. [CrossRef]
87. Zhang, G.; Cen, Q.; Hao, T.; Yin, X.; Zi, X.; Shi, N.; Li, W.; Zhu, N.; Li, M. Self-injection locked silica external cavity narrow linewidth laser. *J. Light. Technol.* **2023**, *41*, 2474–2483. [CrossRef]
88. Mahmudlu, H.; Johanning, R.; Van Rees, A.; Khodadad Kashi, A.; Epping, J.P.; Haldar, R.; Boller, K.J.; Kues, M. Fully on-chip photonic turnkey quantum source for entangled qubit/qudit state generation. *Nat. Photon.* **2023**, *17*, 518–524. [CrossRef]
89. Xu, X.; You, Y.; Hou, J.; Wang, L.; Feng, L.; He, W.; Geng, W.; Liu, Y.; Chou, X. Ultra-narrow bandwidth and large tuning range single-passband microwave photonic filter based on Brillouin fiber laser. *Opt. Laser Technol.* **2023**, *157*, 108735. [CrossRef]
90. Yang, J.Z.; Gao, Z.Q. A tunable 0.2-1.2-GHz N-path bandpass filter with improved harmonic and out-of-band rejection. *IEEE Trans. Microw. Theory Tech.* **2025**, *73*, 6363–6371. [CrossRef]

91. Ma, Y.; Du, Q.; Zhang, W.; Liu, C.; Zhang, H. A miniaturized bandpass filter with wideband and high stopband rejection using LTCC technology. *Electronics* **2024**, *13*, 166. [CrossRef]
92. Hu, Y.; Ma, K.; Wang, Y.; Wu, Y. A filtering ultra-low-noise amplifier based on HISL platform for *ku*-band satellite communication. *IEEE Microw. Wirel. Technol. Lett.* **2025**, *35*, 718–721. [CrossRef]
93. Liu, Y.Q.; Xu, K.D. A filtering Ku-band MMIC low-noise amplifier for satellite communication. In *2022 IEEE MTT-S International Microwave Workshop Series on Advanced Materials and Processes for RF and THz Applications (IMWS-AMP)*; IEEE: Piscataway, NJ, USA, 2022.
94. Resca, D.; Scappaviva, F.; Biondi, A.; Cariani, L.; Vitulli, F. A Ku band MMIC single chip frequency converter for telecom satellite applications. In *2020 15th European Microwave Integrated Circuits Conference (EuMIC)*; IEEE: Piscataway, NJ, USA, 2021.
95. Lee, W.C.; Tsang, K.F.; Shen, Y.; Chui, K.T. A current bleeding CMOS mixer featuring *LO* amplification based on current-reused topology. *Circuits Syst.* **2013**, *4*, 58–66. [CrossRef]
96. Li, K.; Zhang, M.M.; Li, W.H.; Zhou, W.W.; Yan, S.Q.; Tang, M. Coherent optical-transmission technology based on optical-injection-locking carrier recovery. *Chin. J. Lasers* **2024**, *51*, 1406001. (In Chinese)
97. Jiang, Y.; Sun, Y.; Lin, J.; Xie, S.; Su, M. Multifrequency small-signal model for single-phase grid-tied inverters considering the effect of PWM. *IEEE Trans. Power Electron.* **2024**, *39*, 2128–2139. [CrossRef]
98. Burton, R.S.; Fuchshuber, C.F.; Woodford, D.A.; Gole, A.M. Prediction of core saturation instability at an HVDC converter. *IEEE Trans. Power Deliv.* **1996**, *11*, 1961–1969. [CrossRef]
99. Wang, X.; Zhang, J.; Chan, E.H.W.; Feng, X.; Guan, B. Ultra-wide bandwidth photonic microwave phase shifter with amplitude control function. *Opt. Express* **2017**, *25*, 2883–2894. [CrossRef] [PubMed]
100. Safavi, N.; Qashqaei, M.; Ghasemi, F.; Hosseini, S.E. Microwave photonic phase-/delay-tunable mixer based on OSSB-PolM with ultralow mixing spurs. *J. Light. Technol.* **2021**, *39*, 7636–7645. [CrossRef]
101. Zekri, A.; Abderrahmane, L.H. A PLL frequency synthesizer design for C-band satellite communications. In *Proceedings of the 2023 10th International Conference on Recent Advances in Air and Space Technologies (RAST), Istanbul, Turkey, 7–9 June 2023*; IEEE: Piscataway, NJ, USA, 2023.
102. Xia, X.; Wang, Y. S-band phase-locked loop frequency synthesizer for satellite communication and space applications. In *Proceedings of the 2024 IEEE/MTT-S International Microwave Symposium—IMS 2024, Washington, DC, USA, 16–21 June 2024*; IEEE: Piscataway, NJ, USA, 2024.
103. Fan, B.; Baker, V.; Burgos, R.; El Chamie, M.; Chen, W.; Blasko, V.; Boroyevich, D. Common-source inductance induced voltage overshoot and oscillation in active bidirectional devices. *IEEE Trans. Power Electron.* **2021**, *36*, 13383–13388. [CrossRef]
104. Habibullah, M.; Bhumkittipich, K.N.; Mithulananthan, N.; Sharma, R.; Zare, F. Damping oscillation and removing resonance in a RE based DC microgrids. *IEEE Access* **2021**, *9*, 163516–163525. [CrossRef]
105. Jin, Q.; Feng, Q.; Wang, Z.; Ji, R. Modeling of passive intermodulation in coaxial connectors with ideal and nonideal contacts. *IEEE Microw. Wirel. Technol. Lett.* **2024**, *34*, 1331–1334. [CrossRef]
106. Jin, Q.; Gao, J.; Xie, G.; Flowers, G.T.; Ji, R. A study of the passive intermodulation induced by nonlinear characteristics of RF connectors. In Proceedings of the Sixty-Second IEEE Holm Conference on Electrical Contacts, Clearwater Beach, FL, USA, 9–12 October 2016.
107. Liu, R.; Jin, Q.; Song, M.; Wang, Z.; Feng, Q. A novel passive intermodulation model of coaxial cable assemblies with distributed and point-source nonlinearities. *IEEE Trans. Electromagn. Compat.* **2024**, *66*, 1610–1620. [CrossRef]
108. Bi, L.; Gao, J.; Flowers, G.T.; Wang, Z.; Luo, J.; Wang, W. Impact of multiple insertions and withdrawals, and vibration on passive intermodulation in coaxial connectors. *IEEE Trans. Microw. Theory Tech.* **2023**, *71*, 488–499. [CrossRef]
109. Jin, Q.Y.; Feng, Q.Y. Frequency and power dependence of passive intermodulation in connectors with contact-material nonlinear modeling. *IEEE Microw. Wirel. Compon. Lett.* **2021**, *31*, 207–210. [CrossRef]
110. Bayrak, M.; Benson, F.A. Intermodulation products from nonlinearities in transmission lines and connectors at microwave frequencies. *Proc. Inst. Electr. Eng.* **1975**, *122*, 361. [CrossRef]
111. De Sabata, A.; Ignea, A. Passive intermodulation distortions induced by ferromagnetic materials at GSM frequencies. In *Proceedings of the International Symposium on Signals, Circuits and Systems ISSCS 2013, Iasi, Romania, 11–12 July 2013*; IEEE: Piscataway, NJ, USA, 2013.
112. Vicente, C.; Hartnagel, H.L. Passive-intermodulation analysis between rough rectangular waveguide flanges. *IEEE Trans. Microw. Theory Tech.* **2005**, *53*, 2515–2525. [CrossRef]
113. Henrie, J.J. A Study of Passive Intermodulation in Coaxial Cable Connectors. Ph.D. Thesis, Purdue University, West Lafayette, IN, USA, 2009.
114. Ansuinelli, P.; Schuchinsky, A.G.; Frezza, F.; Steer, M.B. Passive intermodulation due to conductor surface roughness. *IEEE Trans. Microw. Theory Tech.* **2018**, *66*, 688–699. [CrossRef]
115. Holm, R. *Electric Contacts: Theory and Application*; Springer: Berlin/Heidelberg, Germany, 1979.

116. Luo, J.; Gao, J.; Zhuang, W.; Wang, Z. Modeling of passive intermodulation induced by concentrated current density in bent coaxial connectors. *IEEE Trans. Microw. Theory Tech.* **2024**, *72*, 4457–4474. [CrossRef]
117. Yang, H.; Wen, H.; Qi, Y.; Fan, J. An equivalent circuit model to analyze passive intermodulation of loose contact coaxial connectors. *IEEE Trans. Electromagn. Compat.* **2018**, *60*, 1180–1189. [CrossRef]
118. Jin, S.; Kwon, M.; Moon, K.; Park, B.; Kim, B. Control of IMD asymmetry of CMOS power amplifier for broadband operation using wideband signal. *IEEE Trans. Microw. Theory Tech.* **2013**, *61*, 3753–3762. [CrossRef]
119. Malucci, R.D.; Panella, A.P. Contact physics of capacitive interconnects. *IEEE Trans. Compon. Packag. Manuf. Technol.* **2013**, *3*, 377–383. [CrossRef]
120. Malucci, R.D. Stability and contact resistance failure criteria. *IEEE Trans. Compon. Packag. Technol.* **2006**, *29*, 326–332. [CrossRef]
121. Ott, M.; Plante, J.; Shaw, J.; Shaw, J.; Garrison-Darrin, M.; Ott, M.; Plante, J.; Garrison-Darrin, M. Fiber optic cable assemblies for space flight applications—Issues and remedies. In *1997 World Aviation Congress, American Institute of Aeronautics and Astronautics*; AIAA: Reston, VA, USA, 1997.
122. Ott, M.N. Fiber optic cable assemblies for space flight: II. Thermal and radiation effects. In *Photonics for Space Environments VI*; Taylor, E.W., Ed.; SPIE: Bellingham, WA, USA, 1998.
123. Putzar, R.; Schaefer, F.; Lambert, M. Vulnerability of spacecraft harnesses to hypervelocity impacts. *Int. J. Impact. Eng.* **2008**, *35*, 1728–1734. [CrossRef]
124. Putzar, R.; Schäfer, F.; Stokes, H.; Chant, R.; Lambert, M. Vulnerability of spacecraft electronics boxes to hypervelocity impacts. In Proceedings of the 56th International Astronautical Congress of the International Astronautical Federation, the International Academy of Astronautics, and the International Institute of Space Law, Fukuoka, Japan, 17–21 October 2005.
125. Liang, F.; Luo, H.; Zhuang, W.; Liang, Z.; Fan, X.; Chen, S.; Sun, Q. Surface charge decay characteristics of epoxy spacer under space charge accumulation. *J. Phys. D Appl. Phys.* **2025**, *58*, 185501. [CrossRef]
126. Hanson, J.; Koenig, D. Fault arcs effects in cable bundles for space applications in vacuum. *IEEE Trans. Dielectr. Electr. Insul.* **1997**, *4*, 394–399. [CrossRef]
127. Yu, H.; Weng, F.; Fu, Y.; Peng, W.; Zhao, Y.; Wang, Y. Design and optimization of stacked high temperature superconductor cable system for space solar power station. *IEEE Trans. Appl. Supercond.* **2025**, *35*, 5400607. [CrossRef]
128. Sun, Y.; Zhang, Y.; Hole, S.; Zhu, Z.; Yang, L.; Guo, C.; Cao, Z.; Yu, E.; Zheng, X.; Zheng, F.; et al. Pressure wave propagation method for space charge measurement in coaxial geometry. *IEEE Trans. Dielectr. Electr. Insul.* **2018**, *25*, 2139–2146. [CrossRef]
129. Chen, C.; Wang, X.; Lv, Z.; Wu, K.; Cheng, C. An equivalent investigation of space charge for plane samples and coaxial cables under a temperature gradient. *IEEE Trans. Dielectr. Electr. Insul.* **2020**, *27*, 1256–1264. [CrossRef]
130. Chen, C.; Bu, Y.; Wang, X.; Cheng, C.; Wu, K. A comparison of space charge behaviors in coaxial cable and film sample under temperature gradient. *IEEE Trans. Dielectr. Electr. Insul.* **2019**, *26*, 1941–1948. [CrossRef]
131. Qiao, G.; Zhuang, Y.; Ye, T.; Qiao, Y. A digital-twin-based detection and protection framework for SDC-induced sinkhole and grayhole nodes in satellite networks. *Aerospace* **2023**, *10*, 788. [CrossRef]

Disclaimer/Publisher's Note: The statements, opinions and data contained in all publications are solely those of the individual author(s) and contributor(s) and not of MDPI and/or the editor(s). MDPI and/or the editor(s) disclaim responsibility for any injury to people or property resulting from any ideas, methods, instructions or products referred to in the content.